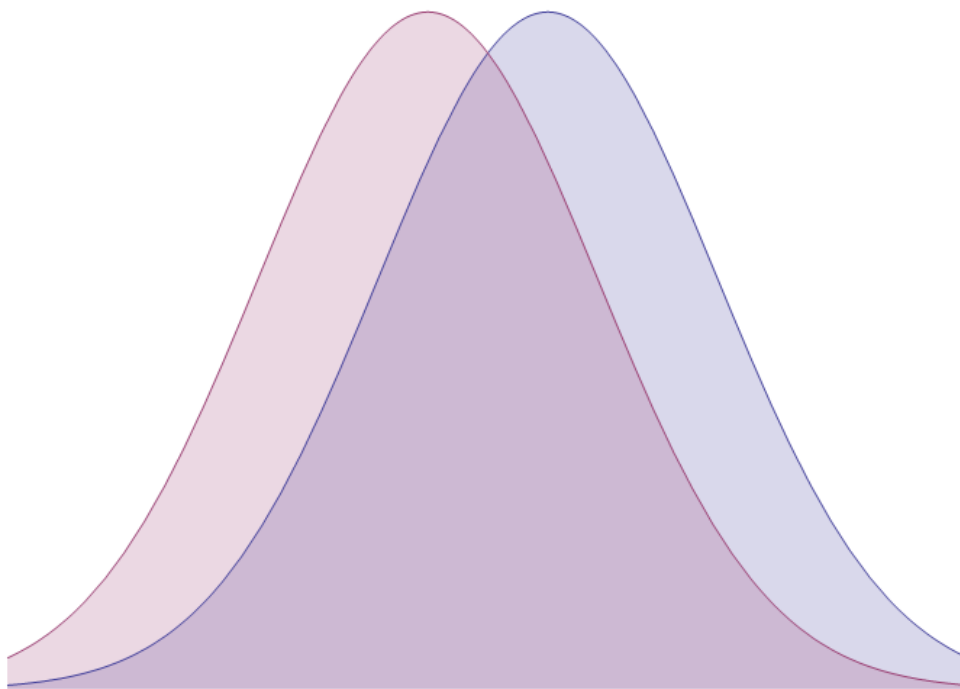# Vernier Scan Analysis

Determining Absolute Luminosity Delivered by RHIC
Run 12 analysis of 500 GeV and 200 GeV $p + p$ collisions

Brookhaven National Laboratory

03 September 2015

University of California, Riverside   **Mike Beaumier**, **Ken Barish**, **Richard Hollis**

STAR Experiment   **K. Oleg Eyser**

Introduction and Executive Summary

The Vernier Scan Analysis is typically done every year, its purpose is to calculate the absolute luminosity of collisions delivered to PHENIX's interaction region (IR) by RHIC. Absolute luminosity is a necessary for the normalization of any cross-section (but not necessary for cross-section ratos).

The vernier analysis is done on a very special data set - obtained during a vernier scan. Unlike normal data taking, PHENIX must use a special trigger configuration optimized for recording very low rates of minimum bias data. The vernier scan itself consists of either the blue, or yellow beams, being incrementally scanned across the other stationary beam. If we assume that the blue and yellow beams are identical, this scan will effecitively show us the transverse dimensions of the blue and yellow beams - these dimenions are used to calculate the luminosity, $\mathcal{L}$, and to verify that our model for relativistic beam collisions is correct.

We can also use the vernier scan to calibrate the Beam Beam Counters (BBC) in order to use them as luminosity monitors. For any BBC trigger, we can represent the relationship between $\mathcal{L}$ and the cross section observed by the BBC as:

$$\mathcal{L}_{BBC} = \frac{R_{BBC}}{\sigma_{BBC}} \tag{1}$$

Where $\mathcal{L}_{BBC}$ is the effective luminosity delivered to a specific BBC trigger, R_{BBC} is the live event rate of the BBC trigger, and σ_{BBC} is defined as the cumulative cross section of events measured by this trigger.

The absolute luminosity is calculated as:

$$\mathcal{L} = \frac{f_{bunch} N_b N_y}{2\pi \sigma_x \sigma_y} \tag{2}$$

Where $\mathcal{L}$ is the luminosity, f_{bunch} is the frequency of each individual bunch crossing, N_b, N_y are the bunch populations for the specific blue and yellow beams, resepectively, and σ_x, σ_y are the transverse widths both bunches in the x and y directions. We assume identical beam bunch distributions for the blue and yellow beams [3], however individual bunches

Run 12 Scanning Patterns
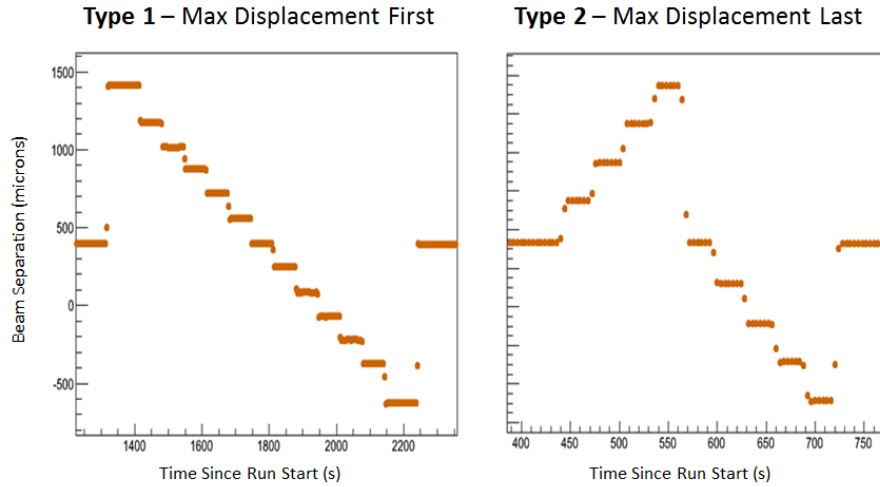
Figure 1: Two different scanning patterns were used in Run 12. Type 2 was previously used in past years prior to 2012, and is included in this year's set of scans as a consistency check. Type 1 was used for the majority of the scans in 2012. The scan order introduces systematic effects based on rate losses in the beam width calculation, which are described later.

can also be studied - and this analysis is presented in this note. f_{bunch} corresponds to the bunch crossing rate of a single specific bunch, and depends on the number of bunches in a specific fill and the blue beam clock.

For clarity: The blue beam clock ticks once every time there is a bunch crossing. Therefore, for 120 bunch fills (including filled and empty bunches), and the standard blue beam clock frequency, f_{clock}, of $9.36MHz$, $f_{bunch} \equiv f_{clock}/120 = 78kHz$.

Previous analysis notes on the vernier analysis are listed below for benefit/curiosity of the reader:

- AN184 [2]

- AN597 [1]

- AN688 [?]

- AN888 [3]

Global vernier scan characteristics are summarized in table 1. Each vernier scan is done slightly differently as a systematic check - beam scan order is varied, beam energy is varied, scan length and step length is varied, and scanning patterns are varied. We expect that these variations will not affect our final result.

Run Number	Fill Number	Energy $(GeV \sqrt{s})$	Scan Time (min)	Scan Pattern	Scan Order	Beam Scanned	Steps	Step Time (s)
359711	16444	200	41	Type 1	H - V	Blue	26	57.5
360879	16470	200	41	Type 1	H - V	Yellow	26	61.2
362492	16514	200	50	Type 1	V - H	Blue	26	62.3
364636	16587	510	58	Type 2	H - V	Yellow	18	21.7
365866	16625	510	53	Type 1	H - V	Blue	26	70.0
366605	16655	510	54	Type 1	H - V	Yellow	26	67.7
367138	16671	510	54	Type 1	H - V	Blue	26	68.65

Table 1: A summary of vernier scans in run 12

Contents

Chapter 1

Variables and Calculations

Though the process of extracting the variables presented in this chapter can sometimes require several steps (or even its own chapter) we present the variables in this chapter from a physical standpoint.

These variables characterize the dynamics of the beams intersecting in the PHENIX interaction region (IR). Our goal in the vernier analysis is to calculate the effective detector cross section for our Beam Beam Counter (BBC) photomultiplier tube detector, as well as the RHIC machine luminosity, $\mathcal{L}_{RHIC}$. We must also use a realistic model for highly relativistic collisions between two intersecting beams.

The basic equations, models and variables used in the analysis are summarized here; no derivations will be provided (but they will be referenced for the interested reader). I will go into detail discussing the extraciton of each parameter within relevent chapters.

The effective detector cross section [4] can be expressed as:

$$\sigma_{ZDC}^{eff} = \frac{R_{max}2\pi n_B n_Y \sigma_x \sigma_y}{n_{bunch} f_{bunch} N_B N_Y} \tag{1.1}$$

with various parameters are defined in Table 1.1.

We use the standard relativistic intersecting beam model for colliding bunches [**?**], which is defined to be:

$$\mathcal{L} = \frac{n_{bunch} f_{bunch} N_B N_Y}{2\pi^2 \sigma_x \sigma_y \sigma z^2} \int \int e^{-\left(\frac{z^2}{\sigma_z^2} + \frac{c^2 t^2}{\sigma_z^2}\right)} c dt \tag{1.2}$$

Variable	Description	Units	Dimension
σ_x, σ_y	bunch profile width obtained from vernier scan beam overlap in x and y directions.	μm	*length*
σ_z	bunch profile width in z-direction, i.e. z-beam width.	μm	*length*
$\dot{N}$	Live event rate for "BBCLL1($>$0 tubes)" trigger	Hz	$time^{-1}$
R_{max}	Maximum BBC Rate determined from maximum overlap of beams rate for "BBCLL1($>$0 tubes)" trigger	Hz	$time^{-1}$
$\mathcal{L}_{RHIC}$	Absolute luminosity delivered to PHENIX IR from RHIC	$cm^{-2}s^{-1}$	$area^{-1}time^{1}$
σ_{p+p}	Inelastic scattering cross section of proton-proton collisions	cm^{2}	$area^{-1}$
N_b^i, N_y^i	Number of ions in bunch i for the blue (b) beam or yellow (y) beam.	count	
f_{bunch}	Frequency of a specific bunch crossing	Hz	$seconds^{-1}$
k_b	Number of bunches filled in one of the beams (assume identical beams)	count	
σ_{BBC}	Cross section of p+p collisions observed by BBC, uncorrected for efficiency	cm^{-2}	$area_{-1}$
ϵ_{BBC}	BBC efficiency	unitless $[0,1]$	
n_{bunch}	Number of filled bunches in the blue or yellow beam	unitless $[0,120]$	

Table 1.1: These are the variables we use in the vernier analysis. Some variables are extracted directly from the data streams (such as the bbc-rate), while others are calculated from distributions of variables (such as the beam-width, $\sigma_{x,y}$).

Chapter 2

Data Streams

For those familiar with PHENIX software, data structures, and raw data processing, this chapter may be skipped. However, as this note will eventually be part of my thesis, I have gone into detail. For an executive summary list of all data sources used in this analysis, I have provided it here:

- PRDF Data (available on either 1 second intervals, or event-by-event basis)

  - GL1P-0: "BBCLL1($>$0 tubes)"
  - GL1P-1: "CLOCK"
  - GL1P-2: "ZDCLL1Wide"
  - GL1P-3: "ZDCLL1Narrow"
  - event-sequence
  - ATP number
  - epoch time stamp
  - GL1 crossing ID (bunch number)

- BPM Data (available in four second intervals)

  - Sector 7 Blue Beam x position
  - Sector 7 Blue Beam y position
  - Sector 7 Yellow Beam x position
  - Sector 7 Yellow Beam y position
  - Sector 8 Blue Beam x position
  - Sector 8 Blue Beam y position
  - Sector 8 Yellow Beam x position

- – Sector 8 Yellow Beam y position
- – epoch time stamp

- • WCM and DCCT Data (avaialble every few seconds)

  - – WCM population for each bunch
  - – DCCT beam current for blue beam
  - – DCCT beam current for yellow beam
  - – epoch time stamp associated with each field of WCM or DCCT data

- • DST Data

  - – BbcOut Node

    - ∗ BBC pmt tubes fired north
    - ∗ BBC pmt tubes fired south
    - ∗ BBC event z-vertex

  - – ZdcOut Node

    - ∗ ZDC event z-vertex

  - – TrigLvl1 Node

    - ∗ bitmasked triglive
    - ∗ bitmasked trigscaled
    - ∗ bitmasked trigraw

  - – SpinDataEventOut Node

    - ∗ GL1P crossing ID
    - ∗ event-sequence
    - ∗ GL1P-0: "BBCLL1($>$0 tubes)"
    - ∗ GL1P-1: "CLOCK"
    - ∗ GL1P-2: "ZDCLL1Wide"
    - ∗ GL1P-3: "ZDCLL1Narrow"

The vernier analysis is unique among various PHENIX analyses because it requires that data streams from RHIC machine sources and the PHENIX detector are synchronized. It is also unique in that the data set itself exibits obvious time dependent behavior. This introduces interesting challenges, as PHENIX software generally does not provide tools to deal with time dependent data, and synchronization of PHENIX data with other RHIC data streams is infrequently done; PHENIX and RHIC data streams effectively live in entirely different software universes (post data production), so there is no guarantee of a common key which can be used to synchronize the data, once we have obtained it.

Previous analyses have generally dealt with each data stream separately, combining only when absolutely neccessary. This approach favors simplicity, but is generally hard to generalize to any data set from any year. PHENIX data sets are generally analyzed as a phase-space data set, with no desire to understand or account for time dependant effects. However, the vernier analysis is intrinsically a time-dependent analysis, so it makes intuitive sense to do the analysis in a way which mirrors the physical process of the vernier scan.

Unfortunately, this means that for portions of the analysis, one must resort to using raw PHENIX data, which incidentally, is not too difficult, it just requires a small amount of custom software to be written.

By understanding the data structures which are available, I have written software (with huge thanks to Joe Seele and Martin Purschke for help with this) which can generally cross check and reproduce any vernier analysis that has been undertaken in previous years, and this has been exploited to provide fast cross-check for the Run 15 vernier analysis. In fact, as it turns out, thanks to the Common-Device (CDEV) data packet contained in PHENIX Raw Data Format files, we can effectively do the analysis starting from the PRDF packet level to achieve total data synchronization. This makes the process of synchronization much easier, as well as reproducing the various data sets from raw data (if avaialble) more straight forward.

Some data is subject to correction for various systematic issues. Those corrections are summarized in the Chapter 4, but are not discussed in detail here.

2.1   Beam Position Monitors

There are two beam position monitors BPM(s) located about 8 meters away from the PHENIX IR on either side (BPM sector 7, and BPM sector 8). The BPMs may be used to establish teh relative separation of the blue and yellow beams, but are not good for establishing absolute beam position [4]. The beam position monitors are coupled capacitavely to the beam pipe(Figure 2.1), with pick ups on the left and right of the pipe, and pickups above and below the pipe. Every four seconds, data is read out from the BPMs. We are given an x and y position, plus an epoch time stamp associated with the blue and yellow beams, from sector 7 and sector 8 respectively. We can geometrically extrapolate the intersection of the blue and yellow beams respectively in the PHENIX IR plane, and then calculate the net separation between the two beams, Figure 2.2.

The BPM data obtained contains measurements of beam position over the course of an entire fill, containing a vernier scan. We use the start and end run times to isolate a chunk of BPM data corresponding to the vernier scan. The data set contains the following fields:

- epoch time
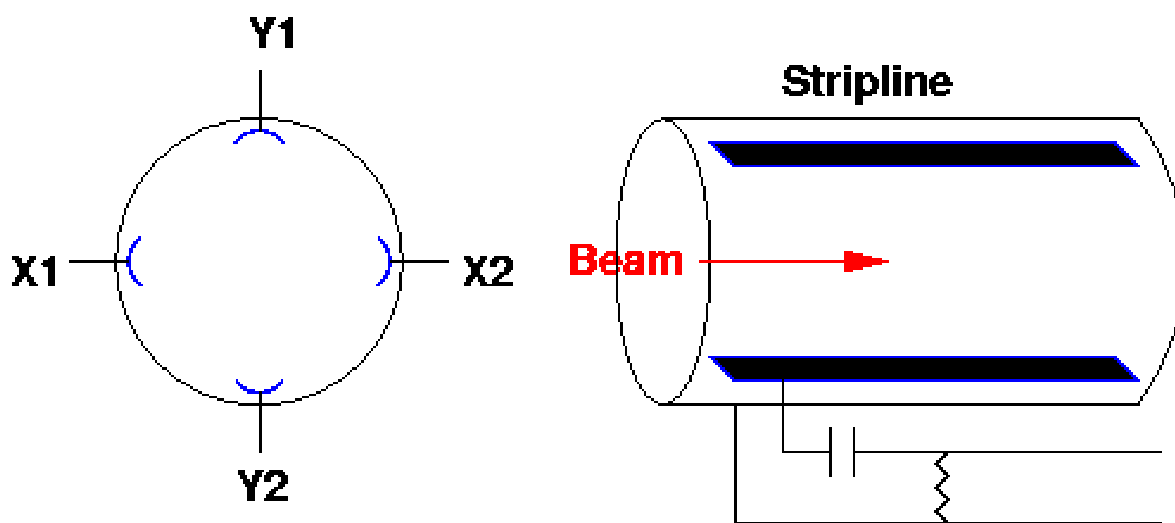
Figure 2.1: Beam Current induces a time dependent voltage proportional to the derivative of the beam current itself. BPM electronics use a comparator circuit, and the readings from X1/2 and Y1/2 to determine the X and Y beam positions. The absolute measurement of beam position is subject to offsets stemming from various effects, however, relative positions (say of one beam to another) are reliable. [**?**]

- blue beam, sector 7 x position

- blue beam, sector 7 x position

- blue beam, sector 8 y position

- blue beam, sector 8 y position

- yellow beam, sector 7 x position

- yellow beam, sector 7 x position

- yellow beam, sector 8 y position

- yellow beam, sector 8 y position

2.2   PHENIX Raw Data Format

The PHENIX raw data format (better known as PRDFs) are the form that recorded data takes immediately after being assembled into events, by the PHENIX DAQ. PRDF data

$$x_{IR} = x_{sector\ 7} + \frac{1}{2}(x_{sector\ 8} - x_{sector\ 7})$$

Use measurements at BPM7 and
BPM8 to produce intersection point
at IR plane of blue, yellow beams.

$$y_{IR} = y_{sector\ 7} + \frac{1}{2}(y_{sector\ 8} - y_{sector\ 7})$$

Blue beam

x

s

z

Yellow beam

Then, once intersection points are
known, calculate distance between
beams, s, at the IR plane.

BPM
Sector 7 Plane

PHENIX Interaction
Region Transverse Plane

BPM
Sector 8 Plane

Figure 2.2: We define three parallel planes, each plane is perpendicular to the beam axis. The planes are at the Sector 7 BPM, the PHENIX IR, and Sector 8 BPM. We assume that the two BPM planes are equidistant from the PHENIX IR. We can geometrically solve for a three dimensional line intersecting all three planes, since we have access, for each beam, intersection points for a given beam at Sector 7 and Sectro 8. With this information, we determine the intersection points in the transverse plane in the PHENIX IR, and then use the two intersection points at the IR plane of the blue and yellow beams to calculate relative beam separation, in both horizontal and vertical directions.

is archived soon after being generated on the massive robotic tape filesystem. PRDF data is hierarchichal, first being organized by event-type, and then organized by packet-type. Every packet has a header, which contains general information such as what the packet contains, and in what order that packet was recieved. Every packet recorded can be associated with a unique event-sequence number, which specifies roughly the order in which the event owning the packet was recieved by the DAQ. Within a given run number, an event-number is guaranteed to be unique. The complexity of the packet is limited by the bandwidth available to move data off PHENIX onto other storage, and the buffers/reconstruction ability of the front end electronics modules built onto PHENIX subsystems.

Generally, raw PHENIX data is too complex to use straight-away, because minimal to no reconstruction of physical properties for a certain event is done (and this varies by the subsystem, and hardware constraints of the subsystem). However, for the vernier analysis, we are generally only interested in very, very simple properties of an event, all of which are completely avaialble directly from the PRDF. This allows us a huge flexibility, as other then the libraries required to dump packet information from PRDFs (i.e. the Event.h) headers, there are no dependancies for obtaining the data we need from PRDFs.

One constraint of using PRDFs as a primary data source is that disk space becomes a constraint. A normal physics run may be segmented into hundreds of PRDFs, each at 20 GB in size. However, because the event rates are on average, quite low for a vernier scan, and because vernier scans typically do not last longer than 20 minutes, there are typically only five or six PRDFs needed to store an entire scan, but in general, using PRDF data without tested data recustruction libraries requires careful checking of the final product.

The data extracted from PRDFs is summarized in table 2.1.

2.2.1   GL1-1P Scalers, ATP Numberand Event Time Stamps

The DAQ supports 32 possible triggers, which may be designed to be arbitrarily sensititve to arbitrary hardware signal coincidences. When PHENIX experiences a trigger, all PHENIX detector subsystems dump the FEM buffers to a the sub-event builders (SEB) which reconstruct raw events, and then pass these events along to the ATPs (Assembly and Trigger Processor) to compress and assemble the events into PRDFs. Over the course of this process, the event is categorized by event type (here, we are concerned with "DATAEVENT" and "SCALEREVENT" types), tagged with a number ($0 \leq ATPNUMBER < 64$), corresponding to the ATP which processed the event, and given an epoch time-stamp. Since time is synchronized between the ATPs via the network, there may be some latency, and these time stamps must be corrected for an offset. Because of the large volume of data, several thousand events will arrive for processing simultaneously, so we can simply choose an ATP (I choose "0") and correct all other time offsets of other ATPs relative to this time, such that we obtain a time offset that we can use to synchronize all epoch times to within one second accuracy for the entire data set.

Other data that are extracted from PRDFS (besides ATPNUMBER, EPOCHTIME, RUN-NUMBER, and EVENTNUMBER) are BUNCHNUMBER, and the GL1-1P scalers.

GL1-1P Scalers are unique counters which may be programmed to track any arbitrary trigger. These counters count the number of "live" triggers for each programmed triggers which occur between recorded events. Each time an event is recorded, the counter dumps the number of "in between" triggers to the GL1P packet. For Run 12, the triggers programmed into the GL1-1P boards were:

- BOARD-ID: 0, "BBCLL1($>$0 tubes)"

- BOARD-ID: 1, "CLOCK"

- BOARD-ID: 2, "ZDCLL1Wide"

- BOARD-ID: 3, "ZDCLL1Narrow"

Generally, to obtain a rate for these trigger scalers, we have two options:

1. Sum all scalers associated with a single EPOCHTIME to get that scaler's per second rate

2. Take the ratio of a particular scaler to the "CLOCK" scaler, converting to a rate using the clock frequency ($9.36MHz$).

Generally the two options should yield the same results, unless there are DAQ issues related to live time. Since this is generally the case, item 2 is generally the preferred method, though there are other methods for correcting for live time. For example, one can use raw events counters, which are contained in "SCALEREVENT" packets and find the ratio between those events and live events contained in "SCALEREVENT" packets.

2.2.2   Scaler Events

Scaler events are a special type of event which tracks the total number of times each one of the 32 triggers has fired. These counters are naturally extremely large numbers, and are avaialble for access in scaler events which are produced once every four seconds. Using these counters can be useful for calculating live time, as we get both live trigger sums and raw trigger sums for all 32 bits. These scalers are used in the Run Control Log to generate overall statistics for each PHENIX run, but many don't realize that we have nearly real-time access to these coutners at the PRDF level.

Source	Field	Description	Application
Event Header	EPOCHTIME	Standard unix time	Time ordering data, Calculation of real-time GL1-1P scaler rates
	ATPNUMBER	ID for ATP handling this event	Synchronization of EPOCHTIME for all events
	RUNNUMBER	Standard PHENIX run ordering	
	EVENTNUMBER	Unique identifier showing order in which DAQ processed events	Unique sorting key, proxy for time
Packet 140008	GL1-1P 0	"BBCLL1(>0 tubes)"	Counts live events between recorded events
	GL1-1P 1	"CLOCK"	""
	GL1-1P 2	"ZDCLL1Wide"	""
	GL1-1P 3	"ZDCLL1Narrow"	""
Packet 140001	Gl1-Crossing ID	Identify bunch crossing	Used to track beam width, σ_{BBC} for specific bunches

Table 2.1: Data extracted from PRDFs.

Node	Description
BbcOut	Number of north/south photo-multiplier tubes fired, and BBC event z-vertex
ZdcOut	Zdc event z-vertex
TrigLvl1	Bitmask for live-events, raw-events and scaled-events.
SpinDataEventOut	Event-sequence, gl1crossing ID (bunch number), four gl1-1p scalers

Table 2.2: A brief summary of data-nodes which are used in the vernier analysis, via DST

2.3   Data Summary Tape

Data Summary Tapes (more commonly referred to as DSTs) are reconstructed data files generated from PRDFs. They are one of the several filetypes generated when PRDFs-events are reconstructed and/or processed. Generally, these files are simply ROOT files which contain trees, historgrams, or specialized classes used to serialize and organize data. The primary advantage of using DSTs is that the file size is small relative to PRDFs, and that there is some amount of consistancy in the way that all DSTs are produced. DSTs are often further reduced to simple ntuples, via Fun4All. The PHENIX Fun4All data reconstruction framework also handles the reduction of PRDFs to other data agglomerations.

The vernier analysis uses its own special data production, and uses the following analysis nodes (Tabel 2.2).

Rates have been extracted and cross checked against rates which are found in PRDFs, and they are identical. The analysis currently only uses the DSTs for calculation of the BBC efficinecy. This will likely not change, because we want to calculate the efficiency of various flavors of minimum bias triggers in this analysis, and this requires that we look at other runs, which contain hundreds of segments.

2.4   Wall Current Monitor and Direct-Current Current-Transformer

The wall current monitor and direct-current current-transformers (WCM and DCCT, respectively) allow us to use induced image-charges in plates capacitively coupled to beam current to calculate the total number of ions in the blue and yellow beams (most accurately using DCCT) and determine individual bunch populations (WCM). Since the DCCT is more accurate, it can be used to calibrate the overall values of bunch populations after summation.
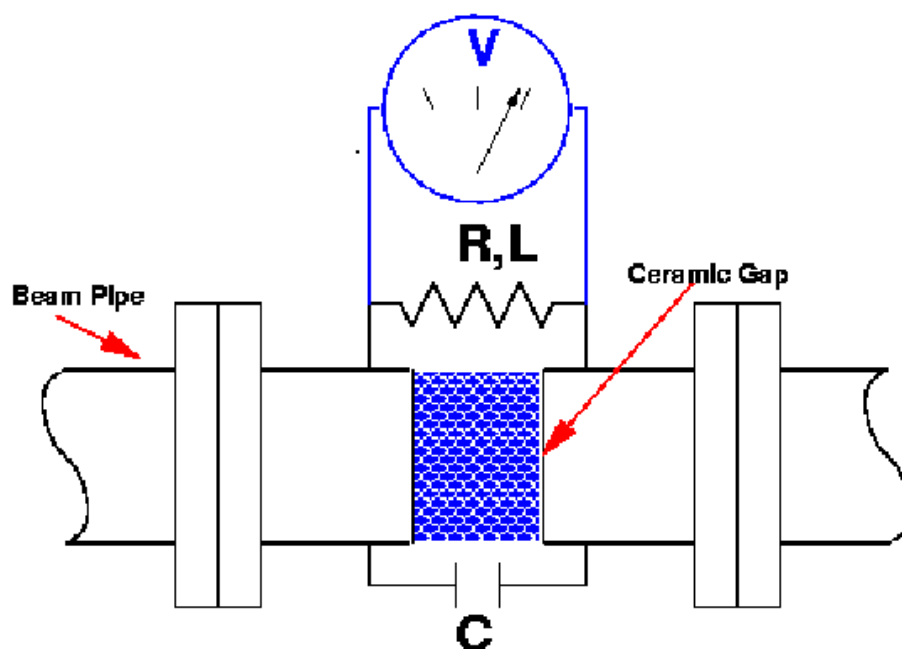
Figure 2.3: Here we see an insulating ceramic break in the beam pipe, which shunts image wall currents from the beam pipe around the toriud. Magnetic shielding excludes external magnetic fields. [**?**]

Like the BPM data, WCM and DCCT data can be in principal accessed from the CDEV packet in PRDFs, however, the framework for doing this has not been developed, as the data streams were parsed from log files and data bases at the time of the various vernier scans.

2.5   Software Repositories

I've developed a suite of software tools which deal with various data streams and analysis segments. The code is extensively documented, so I show its location in CVS here using broad strokes.

I use the PHENIX CVS repository to contain my vernier analysis code. All of my vernier analysis code can be found at: offline/analysis/beaumim/vernierScan .

Relative to this repository root, I have roughly subdivided the other repositories within this root according to the basic tasks it handles.

- vernier_analysis

    - Uses output from vernier_DST_reduction as input
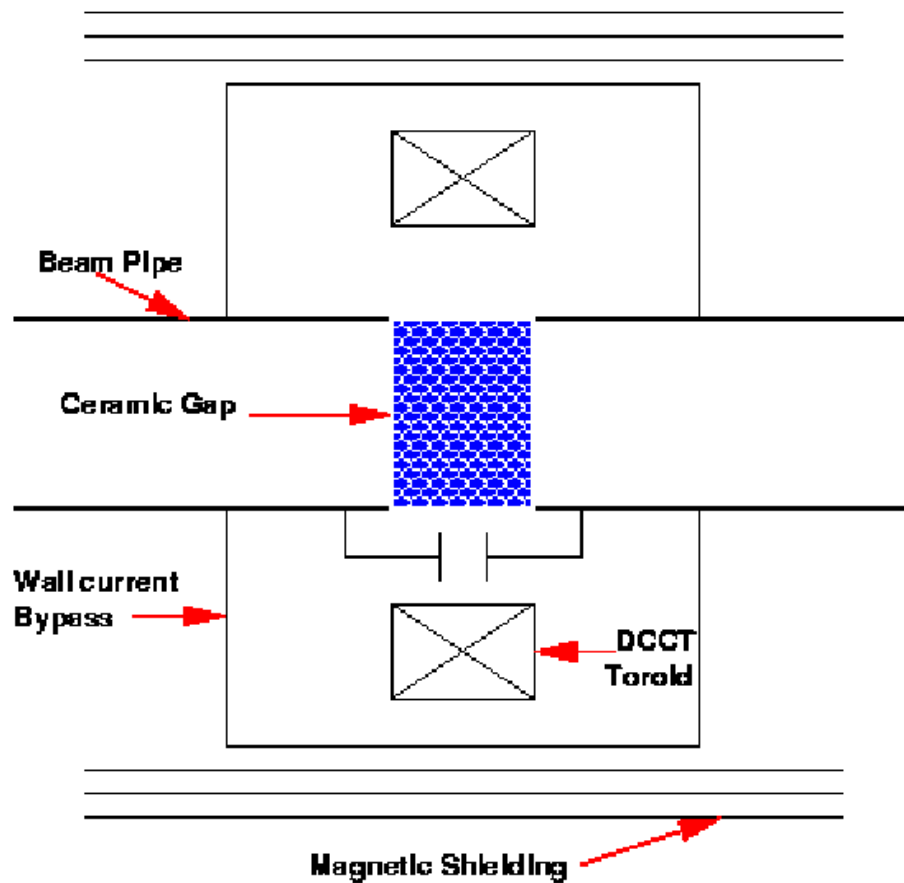
Figure 2.4: The wall current monitor uses an insulating ceramic break in the beam pipe similarly to the DCCT, which forces image wall currents through electronics which measure the current frequencies. The WCM is sensitive only to bunched beams, and can measure longitudianl profiles of bunches [**?**].

- – Beam Width
- – BBC Rate Calculation
- – BPM Data Visualization
- – BBC Efficiency
- – Parameterization of Vernier Scan Steps

- • prdf_analysis

  - – prdf_tools/full_prdf_scalers
    - ∗ Dumps gl1p, bunch, atp and time stamp from PRDF to text file
    - ∗ corrects time stamp
    - ∗ merges PRDF dumps into single file
    - ∗ projects prdf data dumps into bunch integrated, and bunch separated data sets, summed down to indivudual time stamps

  - – prdf_tools/scalers
    - ∗ Reads a PRDF and dumps raw and live scalgger scalers relevant to the vernier analysis. Does scaler overflow corrections.

  - – prdf_tools/processing
    - ∗ Processes BBC Rates
    - ∗ Processes Beam Position
    - ∗ Beam Width

- • vernier_DST_reduction

  - – Reads DSTs and outputs root files with histograms and tree

Chapter 3

Beam Position Monitoring

The Beam Position Monitors (BPMs) have played an important role in this analysis, and in past analyses. They are the one means by which we can directly measure the approximate transverse location of the beams. There are two sets of BPMs on either side of the PHENIX IR, which we call "sector 7" and "sector 8". From these measurements, we can reconstrcut the separation of the blue and yellow beams during a vernier scan. Our purpose in doing so, is to correlate the beam displacement, to the event rate measured by the BBCs, in order to directly measure the width of the beams in the x and y directions (assuming the PHENIX standard coordinate system) **missing-fig phenix coordinate system**. CAD executes these beam displacements through using DX magnets which deflect the beams. The beams follow a planned presciption of movement, and are stepped into, and out of alignment while PHENIX records data.

Past analyses have assumed that the data from the BPMS are unreliable. At times, the polarity of the BPM measurement is flipped from the polarity of the planned step. Regardless, we can use the BPM measurement to obtain a set of beam displacements, and correlate those displacements with time, and with the BBC Rates using PRDF data, so the utility is not insignificant. We can also identify which beam is scanned first from the BPM data and the timing of each step. We can simply substitute planned step displacements if we don't trust the value of beam displacements. We can see summarized the difference betweeen planned steps, and real steps summarized in tables **missing-tab plannedsteps**

CAD_x $(10^{-5}m)$	BPM_x $(10^{-5}m)$	Δ_x (%diff)	CAD_y $(10^{-5}m)$	BPM_y $(10^{-5}m)$	Δ_y (%diff)	BPM_{tot} $(10^{-5}m)$	Δ_{tot} (%diff)
-1000.00	-1103.61	(10 %)	0.00	8.07		1103.64	(10 %)
-750.00	-854.70	(14 %)	0.00	10.67		854.77	(14 %)
-600.00	-720.00	(20 %)	0.00	11.86		720.10	(20 %)
-450.00	-567.61	(26 %)	0.00	13.04		567.76	(26 %)
-300.00	-419.25	(40 %)	0.00	14.25		419.49	(40 %)
-150.00	-258.89	(73 %)	0.00	16.00		259.39	(73 %)
0.00	-106.14		0.00	17.32		107.55	
150.00	63.04	(58 %)	0.00	20.89		66.41	(56 %)
300.00	227.11	(24 %)	0.00	21.36		228.11	(24 %)
450.00	391.46	(13 %)	0.00	24.82		392.25	(13 %)
600.00	542.27	(10 %)	0.00	28.10		542.99	(10 %)
750.00	689.36	(8 %)	0.00	30.36		690.03	(8 %)
1000.00	940.39	(6 %)	0.00	34.04		941.01	(6 %)
0.00	-93.96		-1000.00	-1017.07	(2 %)	1021.40	(2 %)
0.00	-94.75		-750.00	-767.29	(2 %)	773.11	(3 %)
0.00	-95.25		-600.00	-620.36	(3 %)	627.63	(5 %)
0.00	-97.21		-450.00	-470.18	(4 %)	480.12	(7 %)
0.00	-98.07		-300.00	-317.89	(6 %)	332.68	(11 %)
0.00	-98.00		-150.00	-158.64	(6 %)	186.47	(24 %)
0.00	-98.60		0.00	14.27		99.63	
0.00	-98.50		150.00	176.64	(18 %)	202.25	(35 %)
0.00	-97.36		300.00	343.18	(14 %)	356.72	(19 %)
0.00	-94.21		450.00	508.79	(13 %)	517.44	(15 %)
0.00	-92.67		600.00	658.70	(10 %)	665.19	(11 %)
0.00	-90.95		750.00	803.25	(7 %)	808.38	(8 %)
0.00	-88.57		1000.00	1063.50	(6 %)	1067.18	(7 %)

Table 3.1: BPM data compared to CAD data for run 359711. Columns are from left to right, we see the CAD planned horizontal beam displacement, the bpm-measured horizontal beam displacement, $||CAD_x| - |BPM_x||$ (to account for polarity flips in bpm), the CAD planned vertical beam displacement, the bpm-measured beam displacement, $||CAD_y| - |BPM_y||$, the total beam separation ($\sqrt{BPM_x^2 + BPM_y^2}$) and the difference between the measured total separation and the CAD planned total separation. Nominally, CAD promises to hold one beam fixed, and scan the other beam. Rows are each scan step planned and measured for the run.

CAD_x $(10^{-5}m)$	BPM_x $(10^{-5}m)$	Δ_x (%diff)	CAD_y $(10^{-5}m)$	BPM_y $(10^{-5}m)$	Δ_y (%diff)	BPM_{tot} $(10^{-5}m)$	Δ_{tot} (%diff)
1000.00	-1002.45	(0 %)	0.00	64.83		1004.55	(0 %)
750.00	-758.34	(1 %)	0.00	64.38		761.07	(1 %)
600.00	-617.17	(3 %)	0.00	64.83		620.56	(3 %)
450.00	-462.77	(3 %)	0.00	63.90		467.16	(4 %)
300.00	-310.67	(4 %)	0.00	65.70		317.54	(6 %)
150.00	-150.77	(1 %)	0.00	64.43		163.96	(9 %)
0.00	14.63		0.00	63.37		65.03	
-150.00	187.85	(25 %)	0.00	63.54		198.30	(32 %)
-300.00	349.90	(17 %)	0.00	63.47		355.61	(19 %)
-450.00	505.68	(12 %)	0.00	63.04		509.59	(13 %)
-600.00	654.33	(9 %)	0.00	64.47		657.50	(10 %)
-750.00	804.53	(7 %)	0.00	63.97		807.07	(8 %)
-1000.00	1049.00	(5 %)	0.00	64.92		1051.01	(5 %)
0.00	28.71		1000.00	-970.71	(3 %)	971.14	(3 %)
0.00	28.00		750.00	-729.57	(3 %)	730.10	(3 %)
0.00	28.63		600.00	-573.67	(4 %)	574.38	(4 %)
0.00	29.43		450.00	-433.07	(4 %)	434.07	(4 %)
0.00	28.16		300.00	-277.50	(8 %)	278.92	(7 %)
0.00	27.40		150.00	-105.50	(30 %)	109.00	(27 %)
0.00	25.23		0.00	62.73		67.62	
0.00	24.37		-150.00	221.73	(48 %)	223.07	(49 %)
0.00	25.08		-300.00	394.88	(32 %)	395.68	(32 %)
0.00	24.96		-450.00	553.11	(23 %)	553.67	(23 %)
0.00	23.71		-600.00	701.89	(17 %)	702.29	(17 %)
0.00	25.25		-750.00	852.71	(14 %)	853.09	(14 %)
0.00	23.27		-1000.00	1105.00	(10 %)	1105.25	(11 %)

Table 3.2: BPM data compared to CAD data for run 360879. Columns are from left to right, we see the CAD planned horizontal beam displacement, the bpm-measured horizontal beam displacement, $||CAD_x| - |BPM_x||$ (to account for polarity flips in bpm), the CAD planned vertical beam displacement, the bpm-measured beam displacement, $||CAD_y| - |BPM_y||$, the total beam separation ($\sqrt{BPM_x^2 + BPM_y^2}$) and the difference between the measured total separation and the CAD planned total separation. Nominally, CAD promises to hold one beam fixed, and scan the other beam. Rows are each scan step planned and measured for the run.

CAD_x $(10^{-5}m)$	BPM_x $(10^{-5}m)$	Δ_x (%diff)	CAD_y $(10^{-5}m)$	BPM_y $(10^{-5}m)$	Δ_y (%diff)	BPM_{tot} $(10^{-5}m)$	Δ_{tot} (%diff)
0.00	39.32		1000.00	1134.03	(13 %)	1134.71	(13 %)
0.00	38.60		750.00	884.00	(18 %)	884.84	(18 %)
0.00	37.77		600.00	735.70	(23 %)	736.67	(23 %)
0.00	36.37		450.00	587.30	(31 %)	588.42	(31 %)
0.00	36.60		300.00	422.33	(41 %)	423.92	(41 %)
0.00	36.03		150.00	264.10	(76 %)	266.55	(78 %)
0.00	35.36		0.00	98.25		104.42	
0.00	35.54		-150.00	-79.54	(47 %)	87.11	(42 %)
0.00	34.79		-300.00	-245.00	(18 %)	247.46	(18 %)
0.00	33.82		-450.00	-399.00	(11 %)	400.43	(11 %)
0.00	33.83		-600.00	-555.93	(7 %)	556.96	(7 %)
0.00	32.50		-750.00	-705.93	(6 %)	706.68	(6 %)
0.00	32.25		-1000.00	-958.38	(4 %)	958.92	(4 %)
1000.00	1074.84	(7 %)	0.00	104.80		1079.94	(8 %)
750.00	832.50	(11 %)	0.00	102.56		838.79	(12 %)
600.00	680.97	(13 %)	0.00	100.27		688.31	(15 %)
450.00	528.89	(18 %)	0.00	97.68		537.84	(20 %)
300.00	367.29	(22 %)	0.00	95.75		379.56	(27 %)
150.00	215.44	(44 %)	0.00	92.94		234.63	(56 %)
0.00	43.07		0.00	90.23		99.98	
-150.00	-123.21	(18 %)	0.00	89.32		152.18	(1 %)
-300.00	-293.20	(2 %)	0.00	88.00		306.12	(2 %)
-450.00	-440.63	(2 %)	0.00	85.10		448.78	(0 %)
-600.00	-597.93	(0 %)	0.00	83.50		603.74	(1 %)
-750.00	-744.61	(1 %)	0.00	82.71		749.19	(0 %)
-1000.00	-990.64	(1 %)	0.00	79.35		993.81	(1 %)

Table 3.3: BPM data compared to CAD data for run 362492. Columns are from left to right, we see the CAD planned horizontal beam displacement, the bpm-measured horizontal beam displacement, $||CAD_x| - |BPM_x||$ (to account for polarity flips in bpm), the CAD planned vertical beam displacement, the bpm-measured beam displacement, $||CAD_y| - |BPM_y||$, the total beam separation ($\sqrt{BPM_x^2 + BPM_y^2}$) and the difference between the measured total separation and the CAD planned total separation. Nominally, CAD promises to hold one beam fixed, and scan the other beam. Rows are each scan step planned and measured for the run.

CAD_x $(10^{-5}m)$	BPM_x $(10^{-5}m)$	Δ_x (%diff)	CAD_y $(10^{-5}m)$	BPM_y $(10^{-5}m)$	Δ_y (%diff)	BPM_{tot} $(10^{-5}m)$	Δ_{tot} (%diff)
200.00	-183.60	(8 %)	0.00	22.50		184.97	(8 %)
400.00	-382.50	(4 %)	0.00	23.50		383.22	(4 %)
600.00	-581.25	(3 %)	0.00	23.33		581.72	(3 %)
800.00	-777.70	(3 %)	0.00	23.80		778.06	(3 %)
0.00	41.30		0.00	25.40		48.49	
-200.00	267.83	(34 %)	0.00	23.17		268.83	(34 %)
-400.00	467.83	(17 %)	0.00	23.00		468.40	(17 %)
-600.00	667.83	(11 %)	0.00	23.42		668.24	(11 %)
-800.00	863.17	(8 %)	0.00	24.00		863.50	(8 %)
0.00	46.70		200.00	-201.50	(1 %)	206.84	(3 %)
0.00	47.92		400.00	-399.75	(0 %)	402.61	(1 %)
0.00	48.58		600.00	-600.50	(0 %)	602.46	(0 %)
0.00	49.60		800.00	-797.20	(0 %)	798.74	(0 %)
0.00	47.10		0.00	26.00		53.80	
0.00	46.42		-200.00	248.58	(24 %)	252.88	(26 %)
0.00	45.67		-400.00	455.33	(14 %)	457.62	(14 %)
0.00	45.33		-600.00	652.75	(9 %)	654.32	(9 %)
0.00	44.92		-800.00	851.08	(6 %)	852.27	(7 %)

Table 3.4: BPM data compared to CAD data for run 364636. Columns are from left to right, we see the CAD planned horizontal beam displacement, the bpm-measured horizontal beam displacement, $||CAD_x| - |BPM_x||$ (to account for polarity flips in bpm), the CAD planned vertical beam displacement, the bpm-measured beam displacement, $||CAD_y| - |BPM_y||$, the total beam separation ($\sqrt{BPM_x^2 + BPM_y^2}$) and the difference between the measured total separation and the CAD planned total separation. Nominally, CAD promises to hold one beam fixed, and scan the other beam. Rows are each scan step planned and measured for the run.

CAD_x $(10^{-5}m)$	BPM_x $(10^{-5}m)$	Δ_x (%diff)	CAD_y $(10^{-5}m)$	BPM_y $(10^{-5}m)$	Δ_y (%diff)	BPM_{tot} $(10^{-5}m)$	Δ_{tot} (%diff)
-600.00	-577.90	(4 %)	0.00	-6.73		577.94	(4 %)
-400.00	-385.42	(4 %)	0.00	-3.75		385.43	(4 %)
-320.00	-305.67	(4 %)	0.00	-2.68		305.68	(4 %)
-240.00	-226.53	(6 %)	0.00	-1.53		226.53	(6 %)
-160.00	-140.53	(12 %)	0.00	-0.53		140.53	(12 %)
-80.00	-50.83	(36 %)	0.00	1.10		50.85	(36 %)
0.00	38.33		0.00	3.87		38.53	
80.00	134.70	(68 %)	0.00	4.23		134.77	(68 %)
160.00	224.25	(40 %)	0.00	5.25		224.31	(40 %)
240.00	308.87	(29 %)	0.00	6.00		308.93	(29 %)
320.00	391.42	(22 %)	0.00	7.13		391.49	(22 %)
400.00	469.58	(17 %)	0.00	8.22		469.66	(17 %)
600.00	665.71	(11 %)	0.00	10.44		665.79	(11 %)
0.00	39.85		-600.00	-629.28	(5 %)	630.54	(5 %)
0.00	39.78		-400.00	-431.41	(8 %)	433.24	(8 %)
0.00	40.08		-320.00	-354.02	(11 %)	356.29	(11 %)
0.00	40.55		-240.00	-269.69	(12 %)	272.73	(14 %)
0.00	41.57		-160.00	-184.77	(15 %)	189.38	(18 %)
0.00	41.75		-80.00	-93.50	(17 %)	102.40	(28 %)
0.00	41.88		0.00	1.69		41.91	
0.00	43.00		80.00	90.91	(14 %)	100.56	(26 %)
0.00	42.57		160.00	184.73	(15 %)	189.57	(18 %)
0.00	41.21		240.00	271.82	(13 %)	274.92	(15 %)
0.00	41.11		320.00	356.32	(11 %)	358.68	(12 %)
0.00	41.69		400.00	437.19	(9 %)	439.18	(10 %)
0.00	42.33		600.00	636.48	(6 %)	637.88	(6 %)

Table 3.5: BPM data compared to CAD data for run 365866. Columns are from left to right, we see the CAD planned horizontal beam displacement, the bpm-measured horizontal beam displacement, $||CAD_x| - |BPM_x||$ (to account for polarity flips in bpm), the CAD planned vertical beam displacement, the bpm-measured beam displacement, $||CAD_y| - |BPM_y||$, the total beam separation ($\sqrt{BPM_x^2 + BPM_y^2}$) and the difference between the measured total separation and the CAD planned total separation. Nominally, CAD promises to hold one beam fixed, and scan the other beam. Rows are each scan step planned and measured for the run.

CAD_x $(10^{-5}m)$	BPM_x $(10^{-5}m)$	Δ_x (%diff)	CAD_y $(10^{-5}m)$	BPM_y $(10^{-5}m)$	Δ_y (%diff)	BPM_{tot} $(10^{-5}m)$	Δ_{tot} (%diff)
-600.00	677.17	(13 %)	0.00	5.79		677.19	(13 %)
-400.00	481.89	(20 %)	0.00	6.56		481.93	(20 %)
-320.00	408.56	(28 %)	0.00	7.94		408.64	(28 %)
-240.00	330.50	(38 %)	0.00	7.45		330.58	(38 %)
-160.00	243.18	(52 %)	0.00	6.07		243.25	(52 %)
-80.00	150.77	(88 %)	0.00	4.47		150.83	(89 %)
0.00	56.41		0.00	4.85		56.62	
80.00	-38.10	(52 %)	0.00	4.97		38.42	(52 %)
160.00	-129.58	(19 %)	0.00	4.68		129.66	(19 %)
240.00	-213.16	(11 %)	0.00	5.05		213.22	(11 %)
320.00	-292.25	(9 %)	0.00	7.75		292.35	(9 %)
400.00	-373.50	(7 %)	0.00	5.88		373.55	(7 %)
600.00	-571.65	(5 %)	0.00	6.93		571.69	(5 %)
0.00	48.52		-600.00	631.83	(5 %)	633.69	(6 %)
0.00	51.12		-400.00	437.19	(9 %)	440.17	(10 %)
0.00	51.72		-320.00	360.19	(13 %)	363.89	(14 %)
0.00	52.21		-240.00	278.79	(16 %)	283.64	(18 %)
0.00	51.40		-160.00	195.13	(22 %)	201.79	(26 %)
0.00	50.93		-80.00	104.20	(30 %)	115.98	(45 %)
0.00	50.89		0.00	10.46		51.96	
0.00	50.97		80.00	-84.63	(6 %)	98.79	(23 %)
0.00	51.15		160.00	-173.54	(8 %)	180.92	(13 %)
0.00	52.15		240.00	-258.91	(8 %)	264.11	(10 %)
0.00	52.56		320.00	-341.56	(7 %)	345.58	(8 %)
0.00	53.44		400.00	-416.78	(4 %)	420.19	(5 %)
0.00	54.71		600.00	-616.50	(3 %)	618.92	(3 %)

Table 3.6: BPM data compared to CAD data for run 366605. Columns are from left to right, we see the CAD planned horizontal beam displacement, the bpm-measured horizontal beam displacement, $||CAD_x| - |BPM_x||$ (to account for polarity flips in bpm), the CAD planned vertical beam displacement, the bpm-measured beam displacement, $||CAD_y| - |BPM_y||$, the total beam separation ($\sqrt{BPM_x^2 + BPM_y^2}$) and the difference between the measured total separation and the CAD planned total separation. Nominally, CAD promises to hold one beam fixed, and scan the other beam. Rows are each scan step planned and measured for the run.

CAD_x $(10^{-5}m)$	BPM_x $(10^{-5}m)$	Δ_x (%diff)	CAD_y $(10^{-5}m)$	BPM_y $(10^{-5}m)$	Δ_y (%diff)	BPM_{tot} $(10^{-5}m)$	Δ_{tot} (%diff)
-600.00	-588.44	(2 %)	0.00	-3.98		588.45	(2 %)
-400.00	-396.78	(1 %)	0.00	-0.12		396.78	(1 %)
-320.00	-319.86	(0 %)	0.00	-0.67		319.86	(0 %)
-240.00	-242.17	(1 %)	0.00	1.89		242.17	(1 %)
-160.00	-158.47	(1 %)	0.00	2.88		158.50	(1 %)
-80.00	-63.33	(21 %)	0.00	3.88		63.45	(21 %)
0.00	35.20		0.00	4.53		35.49	
80.00	135.30	(69 %)	0.00	4.97		135.39	(69 %)
160.00	229.44	(43 %)	0.00	6.00		229.52	(43 %)
240.00	315.29	(31 %)	0.00	7.91		315.39	(31 %)
320.00	396.29	(24 %)	0.00	7.32		396.36	(24 %)
400.00	471.53	(18 %)	0.00	7.69		471.59	(18 %)
600.00	666.17	(11 %)	0.00	10.67		666.25	(11 %)
0.00	38.91		-600.00	-635.34	(6 %)	636.53	(6 %)
0.00	38.59		-400.00	-438.25	(10 %)	439.95	(10 %)
0.00	38.75		-320.00	-359.68	(12 %)	361.76	(13 %)
0.00	39.08		-240.00	-277.36	(16 %)	280.10	(17 %)
0.00	38.77		-160.00	-193.11	(21 %)	196.96	(23 %)
0.00	39.17		-80.00	-96.79	(21 %)	104.41	(31 %)
0.00	41.33		0.00	3.43		41.48	
0.00	41.79		80.00	106.54	(33 %)	114.44	(43 %)
0.00	42.97		160.00	196.62	(23 %)	201.27	(26 %)
0.00	42.50		240.00	282.81	(18 %)	285.99	(19 %)
0.00	41.45		320.00	364.29	(14 %)	366.64	(15 %)
0.00	41.41		400.00	442.75	(11 %)	444.68	(11 %)
0.00	41.38		600.00	642.98	(7 %)	644.31	(7 %)

Table 3.7: BPM data compared to CAD data for run 367138. Columns are from left to right, we see the CAD planned horizontal beam displacement, the bpm-measured horizontal beam displacement, $||CAD_x| - |BPM_x||$ (to account for polarity flips in bpm), the CAD planned vertical beam displacement, the bpm-measured beam displacement, $||CAD_y| - |BPM_y||$, the total beam separation ($\sqrt{BPM_x^2 + BPM_y^2}$) and the difference between the measured total separation and the CAD planned total separation. Nominally, CAD promises to hold one beam fixed, and scan the other beam. Rows are each scan step planned and measured for the run.

Chapter 4

Systematic Corrections

This chapter serves as an introduction to the various corrections which are applied along the analysis chain. In the case where corrections are small, and don't warrant an entire chapter, I will discuss in detail here, but for other correcitons, I will simply introduce here, and devote a whole chapter to them.

4.1   Crossing Angle and β^*: The Hourglass Effect

In the model for beam lumonisty discussed in Equation 2, section (BROKEN REFERENCE), we neglected to mention the importance of the z-dependant ion distributions in each bunch. In fact, beam bunches have a very real z-dependant componant of their ion distributions. If we could view the transverse beam width at various points along the bunch in the z-dimension, we would find that the transverse beam width varied as a function of z. However, because we must trigger our data, our mininmum bias trigger imposes vertex range over which we can observe events. When we measure horizontal and vertical beam widths using the vernier scan technique, we are effectively measuring weighted average horizontal and vertical beam widths over a z-vertex range of 0 to 30 centimeters [**?**]. Suffice to say, we have an incomplete model for our beam gemoetry, and must account for the z-dependance of our bunch density distributions, and we do so using the measured horizontal and vertical beam widths as a constraint.

Chapter 5 discusses this correction in detail.

4.2   Luminosity Losses

Anyone who has been on shift is familiar with the overhead displays of the beam intensity. We all know that as any fill progresses, there is luminosity loss, which will affect the BBC

Rate. Losses in the BBC Rate will skew any distributions that depend on this parameter, and in this analysis, the beam width is such a distribution. Vernier scans are taken towards the end of a fill, since luminosity losses are more extreme at the beginning of the fill. In general, these losses account for about 1 or 2 percent, though they are calculated explicitly in this analysis over the duration of each scan.

NOTE: show how we derive a linear relationship between beam losses and the product of the WCMBlueTotal and WCMYellowTotal, fit this with a line, and then use the fit to correct the BBC rate data

4.3   Beam Position Monitoring vs Planned Scan Steps

4.4   Time Synchronization

Chapter 5

Hourglass Correction

5.1   Introduction

As discussed in Chapter 4, the purpose of determining β^* and θ_{xing} is to correct our luminosity obtained from the Vernier Scan by using a more realistic model of the beams. The reason this correction bears the name "Hourglass Correction" is historical and memetic - the beams when focused in to the IR tend to have the geometry of an hourglass lying on its side, due to the focusing parameter, β^*, which would be symmetrical about the nominal $z = 0$ point at the center of the IR, except for that due to the non-zero crossing crossing angle, θ_{xing}. This is nomrally not visible, when beams are overlapped at $z = 0$, but when beams are displaced, the characteristic shape can be seen by a splitting of z-vertex profile. The two humps gain unequal heights when the crossing angle strays away from zero.

Because the shape of this distriubtion depends on the luminosity integral, we cannot normally fit the z-vertex profile that we obtain from data. However, using a Toy Monte-Carlo, we an simulate the z-vertex profile, then compare the simulated profile using least-squares regression and χ^2 comparisons. The simulation depends on about twenty parameters, which I summarize in Figure 5.4.

The luminosity of two beams consisting of colloding bunches of any geometry is described by the convelution of each bunch density over all four space-time coordinates:

$$\mathcal{L} = 2f_{bunch}n_{bunch}N_{blue}N_{yellow} \int \int \int \int_{-\infty}^{\infty} \rho^{blue}(x,y,z+ct)\rho^{yellow}(x,y,z-ct)2c\,dt\,dz\,dx\,dy$$

$$(5.1)$$
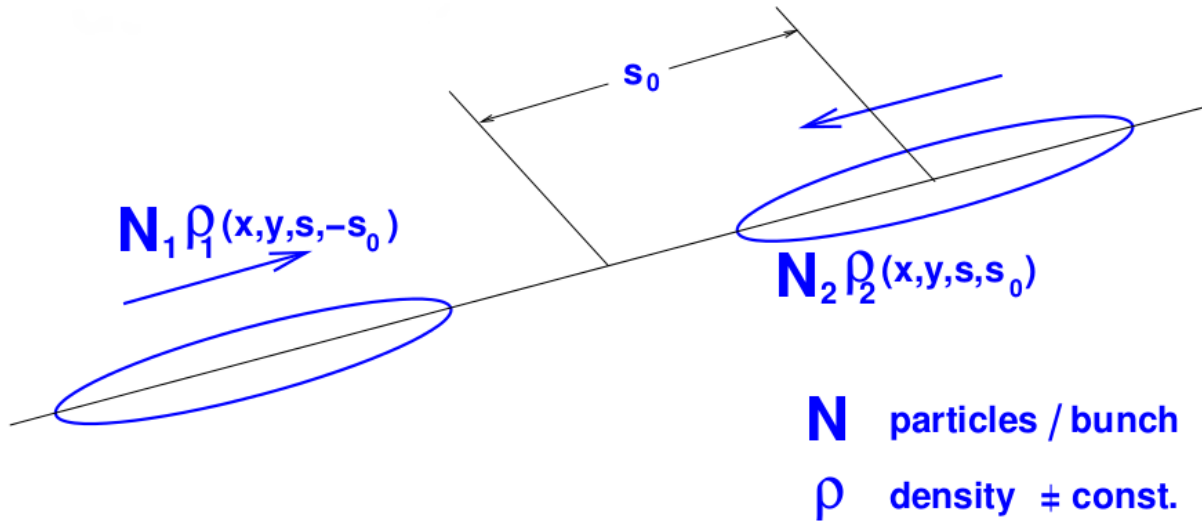
Figure 5.1: Here we see two bunches colliding head on, which is a simplified model used to estimate the expected luminsoity, before the application of the β^* squeezing effect and any existence of crossing angles, θ_{XZ} or θ_{YZ}

5.2   Realistically Modeling the Beam

In simulation, we need to use densities which realistically model the beam's real shape, [?]. We can naievely model the beams in the transverse direction as simple normal gaussian distriubtions (Eq 5.2), assuming head-on collisions (Figure 5.1).:

$$\rho(x_i) = \frac{e^{-\frac{(x_i-\mu)^2}{2\sigma_{x_i}^2}}}{\sigma_{x_i}\sqrt{2\pi}} \tag{5.2}$$

However, equation 5.2 does not capture the true geometry of the beams. We know that there is a β squeeze near the PHENIX IR which squeezes the beam, focusing it into a smaller area before collissions to boost luminosity. We also know that, due the fact that we have intersecting rings, that there may be some small crossing angle between the bunches. Both of these effects, β^* and the crossing angle, affect luminosity. Previous analyses [?] found the β^* effect to modify the luminosity by about 30%, and the crossing angle by about 1%.

Recall from Eq **??** that we have four-dimensional conveluted densities as our integrand for calculation of luminosity. We need to make some simplifying assumptions about the functional form of these densities, and then add in corrections to give us a good estimation

of beam geometry. Firstly, we assume that the densities are seperable, i.e.:

$$\rho(x, y, z \pm ct) \rightarrow \rho_x(x)\rho_y(y)\rho_z(z \pm ct) \tag{5.3}$$

We know that the time-dependence of the luminosity is merely to reflect that the bunches are moving, so there is no "density" in time, from a certain perspective. We simply observe at the IR two bunches passing through eachother (sometimes interacting). This is captured by the $\pm ct$ term in ρ_z.

The z-profile of the beams do not have an obvious analytical description. However, this is not a concern for numerical integration of the luminosity overlap integral. We can generate these profiles using the wall-current-monitor data, which also provides a finely binned data stream - giving us sub-nanosecond resolution on the beam profile in the z-direction. The WCM profile is unique to a fill, though is constrained to fit into the "beam-buckets" which are simply areas of low potential containing bunched ions. Angelika Drees from CAD averaged the profiles for one beam-revolution, and provided them to me. They are plotted in figures 5.6, 5.7, 5.8, 5.9, 5.10, 5.11, and 5.12.

Now, we modify the transverse profiles of tour model in x and y to reflect the β^* squeeze, as well as the crossing angles. The β^* squeeze will modify the transverse beam widths, introducing a z dependance, so we apply this trasformation to our simple bunch model. Crossing angles in the XZ and YZ planes introduce further z-dependance into the x and y bunch distributions, and additionally introduce x and y dependence into the z-profile. The rotation is accomplished with a simple coordinate transform.

$$C_{norm}e^{\frac{-(x-\mu_x)^2}{2(\sigma)^2}} \tag{5.4}$$

Transformation of the beam widths due to β_* squeezing (see Figure 5.3

$$\sigma_i \rightarrow \sigma_i^* = \sigma_i\sqrt{1 + \left(\frac{z}{\beta^*}\right)^2} \tag{5.5}$$

$$i = x, y \tag{5.6}$$

Now apply the rotation, see Figure 5.2:

$$x_{blue} \rightarrow x\cos\frac{\phi}{2} - z\sin\frac{\phi}{2} \tag{5.7}$$

$$z_{blue} \rightarrow z\cos\frac{\phi}{2} + x\sin\frac{\phi}{2} \tag{5.8}$$

$$x_{yellow} \rightarrow x\cos\frac{\phi}{2} + z\sin\frac{\phi}{2} \tag{5.9}$$

$$z_{yellow} \rightarrow z\cos\frac{\phi}{2} - z\sin\frac{\phi}{2} \tag{5.10}$$

$$\sin\frac{\phi}{2} \rightarrow \frac{\phi}{2} \tag{5.11}$$

$$\cos\frac{\phi}{2} \rightarrow 1 + \frac{\phi^2}{4} \tag{5.12}$$

$$x_{blue}^R = x\left(1 + \frac{\phi^2}{4}\right) - z\frac{\phi}{2} \tag{5.13}$$

$$z_{blue}^R = z\left(1 + \frac{\phi^2}{4}\right) + x\frac{\phi}{2} \tag{5.14}$$

$$x_{yellow}^R = x\left(1 + \frac{\phi^2}{4}\right) + z\frac{\phi}{2} \tag{5.15}$$

$$z_{yellow}^R = z\left(1 + \frac{\phi^2}{4}\right) - z\frac{\phi}{2} \tag{5.16}$$

$$\tag{5.17}$$

Rather then write down the final (frankly hideous) form of the luminsoity integral, I will instead write it down in terms of these transformed coordinates.

$$\sigma_i^* \rightarrow \sigma_i^{*R} = \sigma_i\sqrt{1 + \left(\frac{z^R}{\beta^*}\right)^2} \tag{5.18}$$

$$\rho_{x_i}(x_i) \rightarrow \rho_{x_i^R}^*(x_i^R) = C_{x_i} e^{\frac{-\left(x_i^R - \mu_x\right)^2}{2\left(\sigma_i^{*R}\right)^2}} \tag{5.19}$$

$$i = x, y \tag{5.20}$$

$$\tag{5.21}$$

We plug the separable models for density into the luminosity integral to obtain our final form. Although the simple gaussian integration can be normalized ahead of time due to knowlege of that function's total integral, in this case, it may be neccessary to numerically integrate the density functions, and apply an overall normalization.

Φ

$\rho_1(x,y,s,-s_0)$ $\rho_2(x,y,s,s_0)$

x

$x_1 = x \cos\ \phi/2 - s \sin\ \phi/2$

$s_2 = -s \cos\ \phi/2 + x \sin\ \phi/2$

$s_1 = s \cos\ \phi/2 + x \sin\ \phi/2$

$\phi/2$

s

$\phi/2$

$x_2 = -x \cos\ \phi/2 - s \sin\ \phi/2$
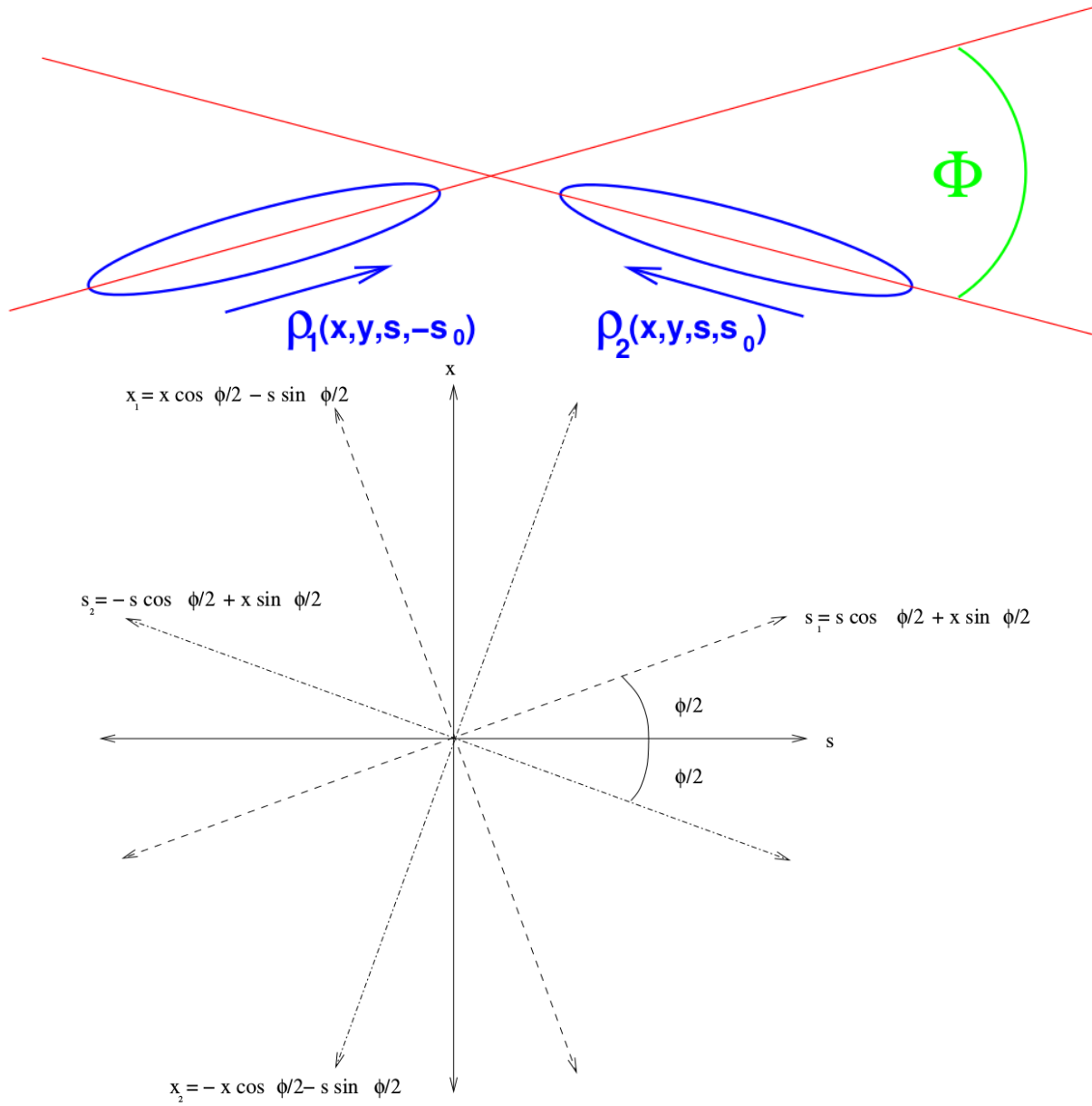
Figure 5.2: Here, we see a schematic view of the coordinate rotation due to the crossing angle (in this case we see the XZ plane, but the situation is identical in the YZ plane).
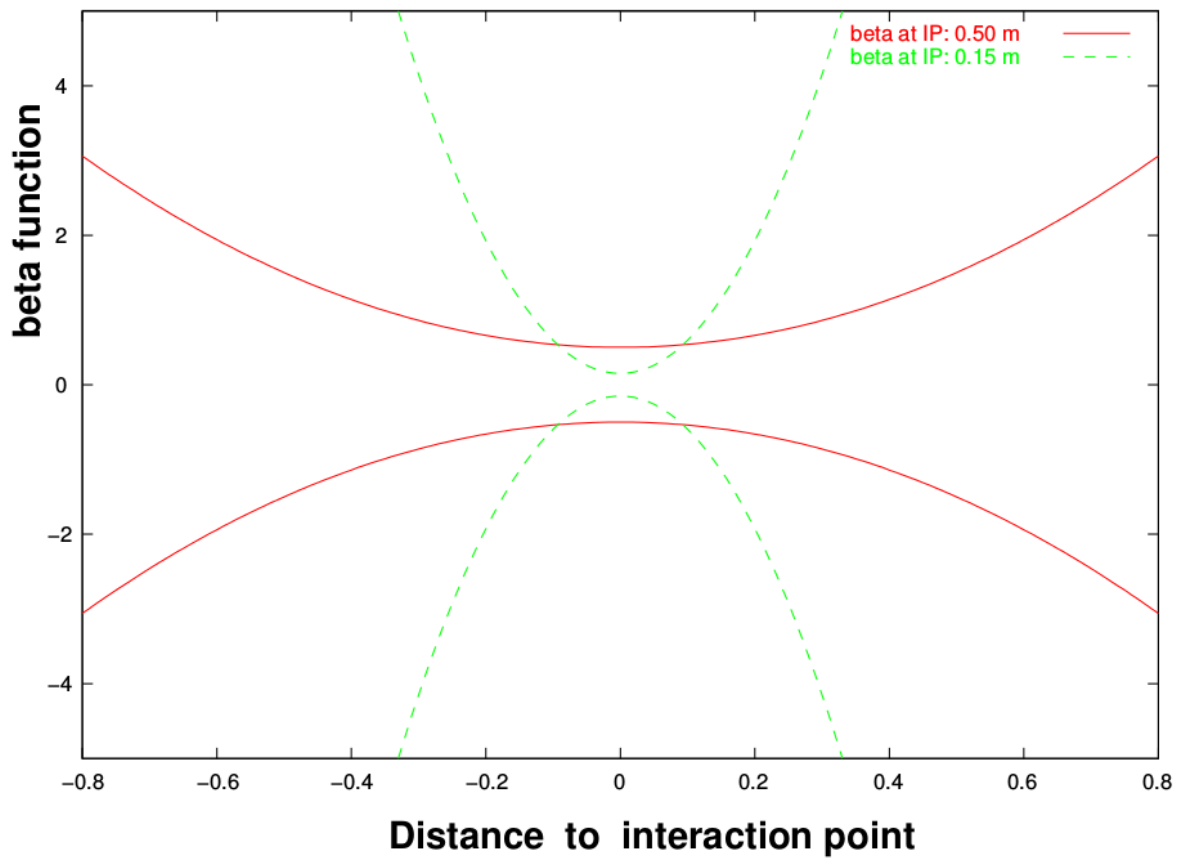
Figure 5.3: Here, we see a function of z, β^*, which shows the shape of the squeezing potential in one of the planes. Two different values of β^* are shown.

```
                  AVG_NUMBER_IONS_BLUE_BEAM 120.029e9
                 AVG_NUMBER_IONS_YELLOW_BEAM 88.1677e9
                   BBC_ZDC_Z_VERTEX_OFFSET -9.53756
                              BETA_STAR 85
                    BUNCH_CROSSING_FREQUENCY 78213.
                      CROSSING_ANGLE_XZ -0.08e-3
                        CROSSING_ANGLE_YZ 0.
                         FILLED_BUNCHES 107
                  HORIZONTAL_BEAM_WIDTH 0.0245674
                           MAX_COLLISIONS 5
                    MULTIPLE_COLLISION_RATE 0.001
                         RUN_NUMBER 359711
                   VERTICAL_BEAM_WIDTH 0.0238342
                            X_OFFSET -0.1
                             Y_OFFSET 0
                          ZDC_COUNTS 592
          ZDC_VERTEX_DISTRIBUTION_NAME zdc_zvtx_step_0
           Z_BUNCH_WIDTH_CENTRAL_GAUSIAN 55.95
            Z_BUNCH_WIDTH_LEFT_GAUSSIAN 35.15
             Z_BUNCH_WIDTH_LEFT_OFFSET -70.2
            Z_BUNCH_WIDTH_RIGHT_GAUSIAN 27.65
             Z_BUNCH_WIDTH_RIGHT_OFFSET 56.7
                Z_PROFILE_SCALE_VALUE 2.0
```

Figure 5.4: Each parameter is initialized directly from data. Parameters which are our goal to determine, β^* and θ_{xing} are obtained from reasonable ranges predicted by CAD, and then varied until good agreement is reached.

5.3   Monte Carlo Simulation and Numerically Integrated Luminosity

The toy Monte Carlo is seeded with initial values which are extracted from the data, and then the parameters are adjusted until suitably matching the data distribution.

Within the toy Monte-Carlo, we calculate the full form of the Luminosity, by making a few simplifying assumptions.

- All bunches are identical

- Beam widths obtained from the vernier scan are good approximations

- Which bunches are filled/unfilled do not matter, so long as we have the correct number of filled bunches.

- There is no crossing angle in the z-y plane, only the z-x plane (this can be verified as a good assumption by observing figure (FIGURE REFERENCE NEEDED)

Once we simulate the luminosity, we compare this to the overall luminosity obtained directly from the data (but without correction for the hourglass effect or crossing angle). We obtain the ratio of the two luminosities, thus yielding our multiplicative correction factor.

Within the simulation, we calculate the luminosity via a riemann sum, binning space and time finely enough to converge to a reasonable value.

The general work flow of the simulation and minimization process is modeled schematically in 5.5.
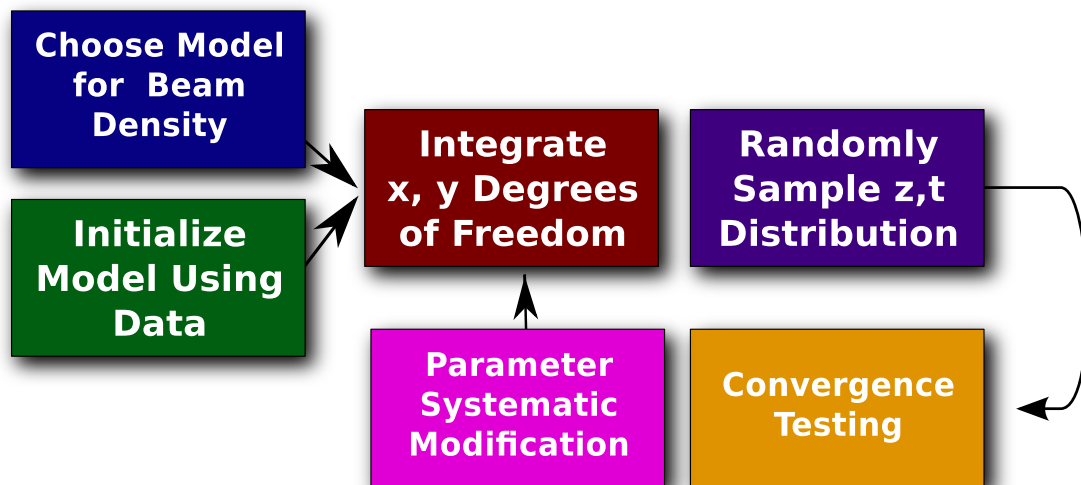
Figure 5.5: Here we see the schematic overview of the simulation. Each box represents a distinct step we take in the modeling or numeric integration of the luminosity. Because we use numeric methods for solving the luminosity integral, we do not have easy access to regression methods such as gradient-descent. Instead we start matching the zdc z-vertex profile with the simulated profile, and then vary the configuration parameters over reasonable ranges, choosing the result which minimizes the difference between the distributions.
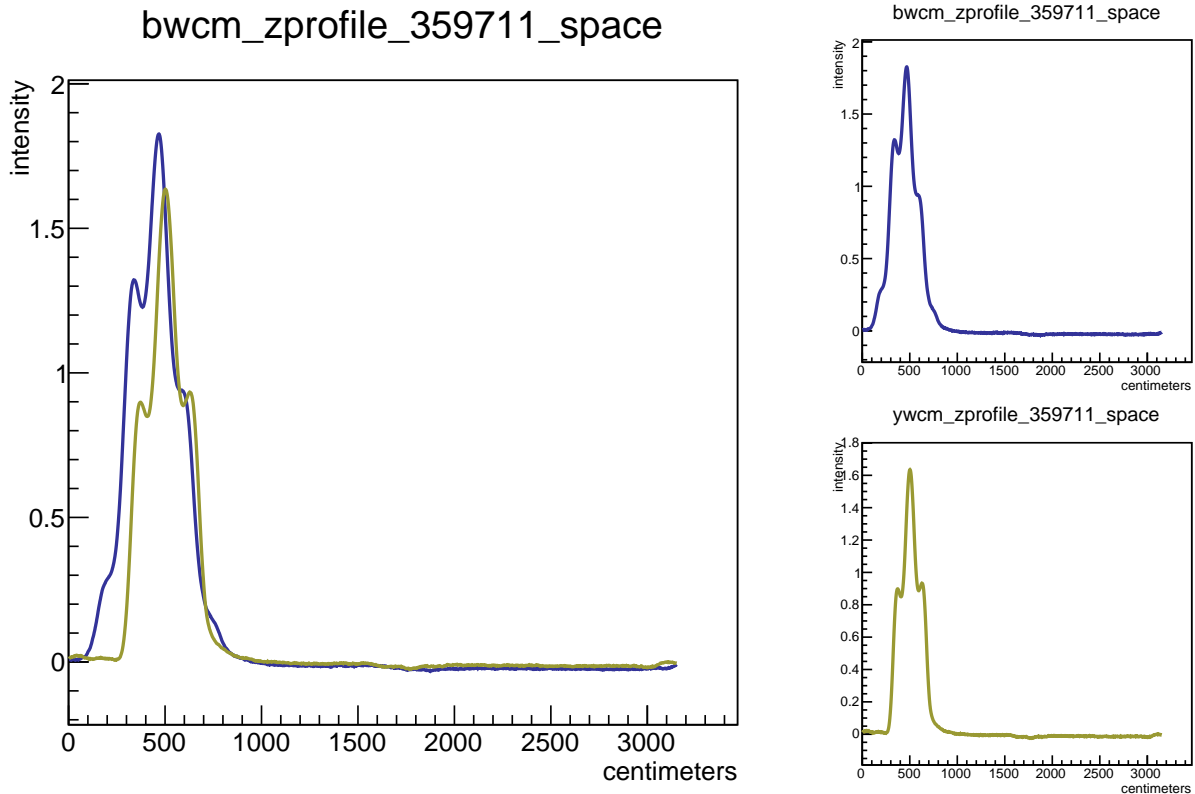
Figure 5.6: Left: the blue and yellow wall current monitor beam z-profiles. One can see the three beam buckets which make up one so-called "filled bunch". Bunches are approximately 1000 cm long, the entire profile passes the IR once every 106 nanoseconds, though most of the bunch is actually within a time envelope of approximately 35 nanosecons. The panes on the right show the blue beam (top) and the yellow beam (bottom).
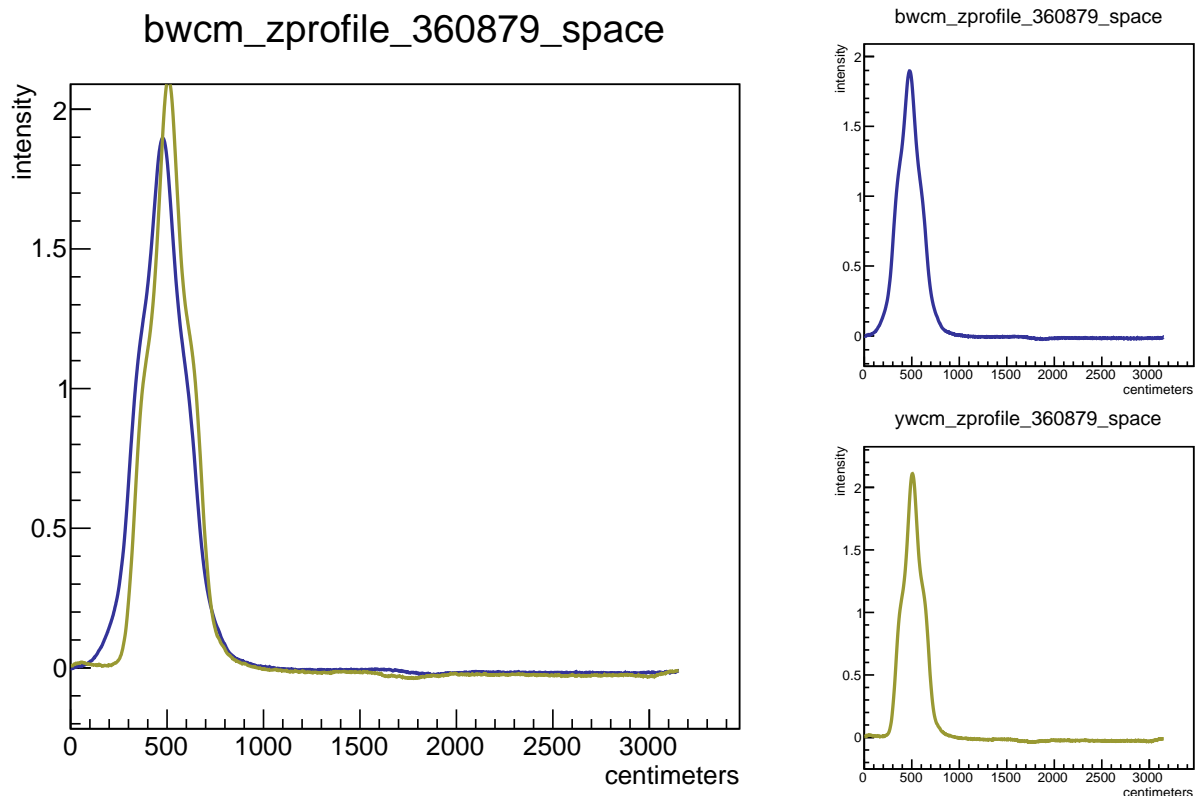
Figure 5.7: Left: the blue and yellow wall current monitor beam z-profiles. One can see the three beam buckets which make up one so-called "filled bunch". Bunches are approximately 1000 cm long, the entire profile passes the IR once every 106 nanoseconds, though most of the bunch is actually within a time envelope of approximately 35 nanosecons. The panes on the right show the blue beam (top) and the yellow beam (bottom).
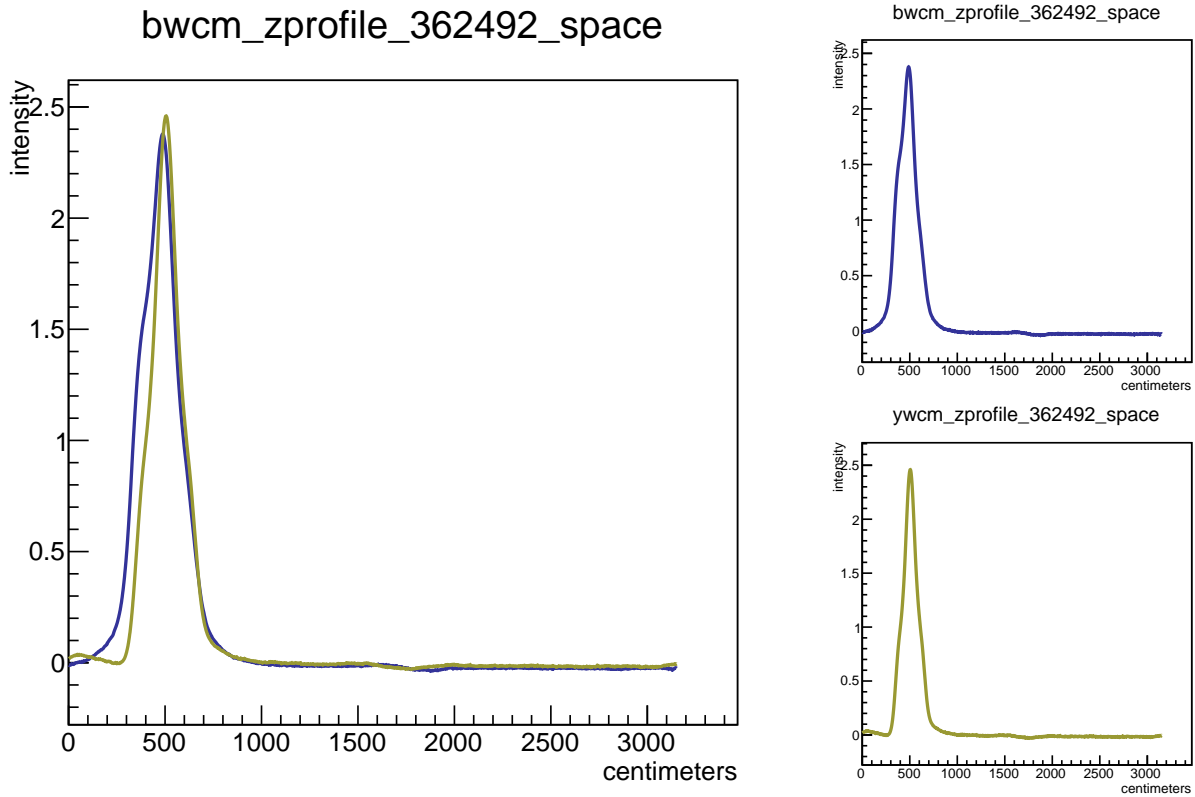
Figure 5.8: Left: the blue and yellow wall current monitor beam z-profiles. One can see the three beam buckets which make up one so-called "filled bunch". Bunches are approximately 1000 cm long, the entire profile passes the IR once every 106 nanoseconds, though most of the bunch is actually within a time envelope of approximately 35 nanosecons. The panes on the right show the blue beam (top) and the yellow beam (bottom).
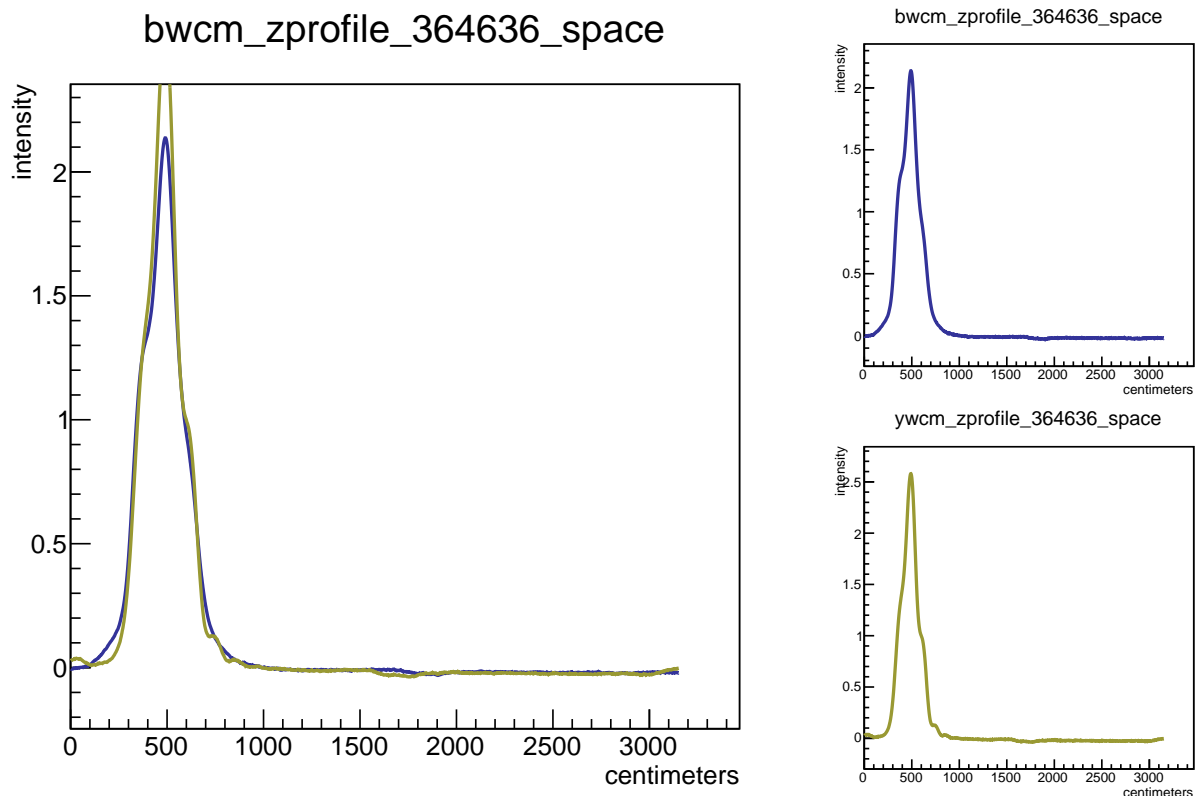
Figure 5.9: Left: the blue and yellow wall current monitor beam z-profiles. One can see the three beam buckets which make up one so-called "filled bunch". Bunches are approximately 1000 cm long, the entire profile passes the IR once every 106 nanoseconds, though most of the bunch is actually within a time envelope of approximately 35 nanosecons. The panes on the right show the blue beam (top) and the yellow beam (bottom).
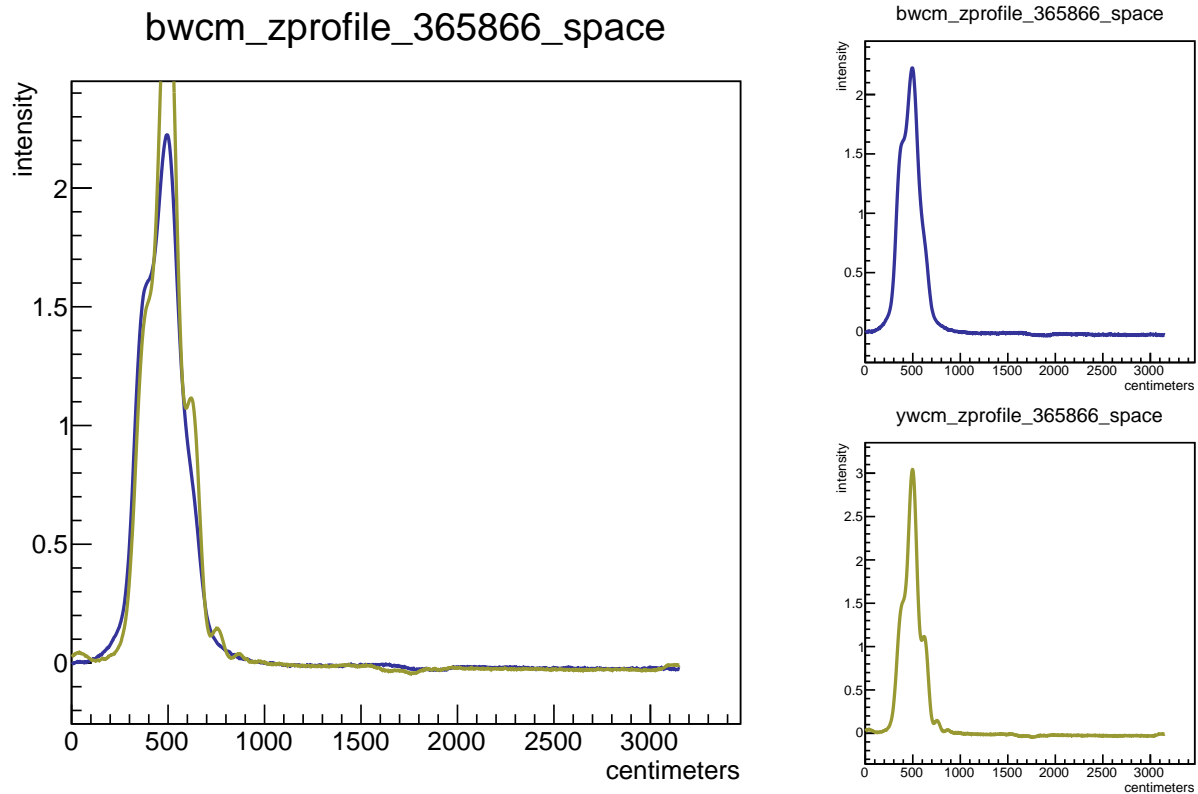
Figure 5.10: Left: the blue and yellow wall current monitor beam z-profiles. One can see the three beam buckets which make up one so-called "filled bunch". Bunches are approximately 1000 cm long, the entire profile passes the IR once every 106 nanoseconds, though most of the bunch is actually within a time envelope of approximately 35 nanosecons. The panes on the right show the blue beam (top) and the yellow beam (bottom).
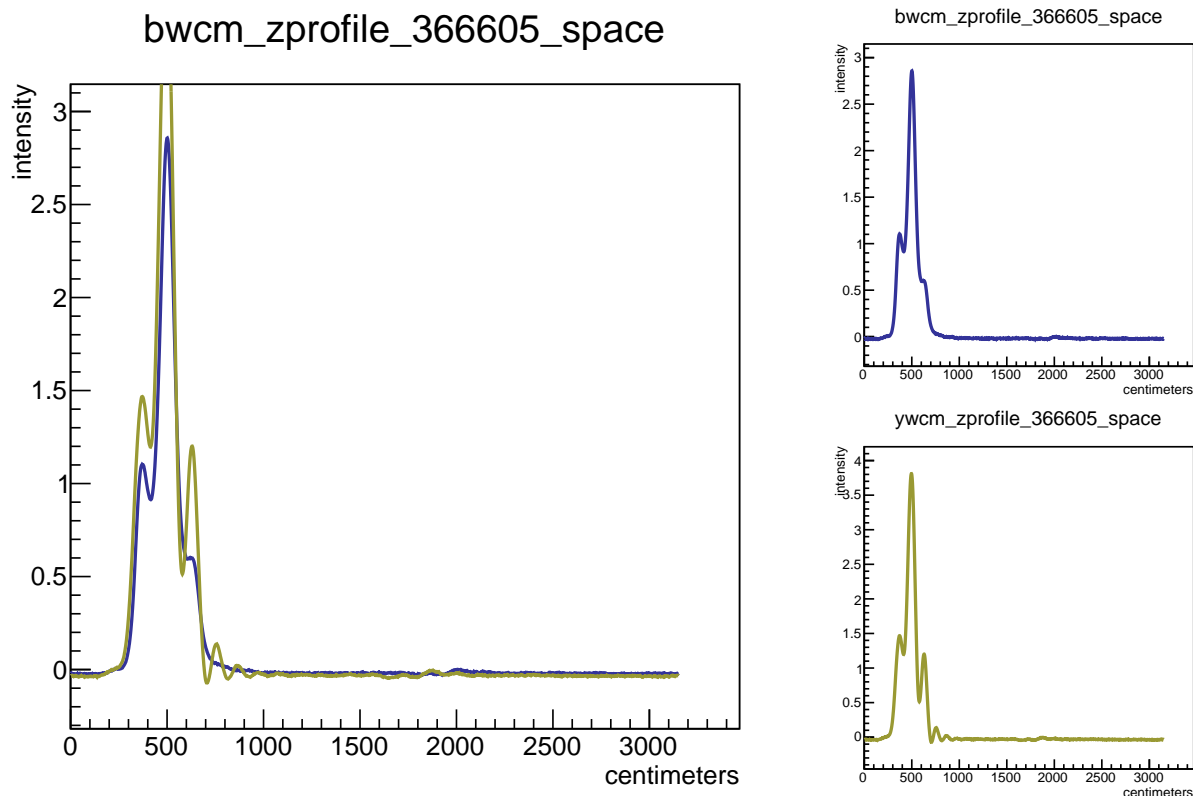
Figure 5.11: Left: the blue and yellow wall current monitor beam z-profiles. One can see the three beam buckets which make up one so-called "filled bunch". Bunches are approximately 1000 cm long, the entire profile passes the IR once every 106 nanoseconds, though most of the bunch is actually within a time envelope of approximately 35 nanosecons. The panes on the right show the blue beam (top) and the yellow beam (bottom).
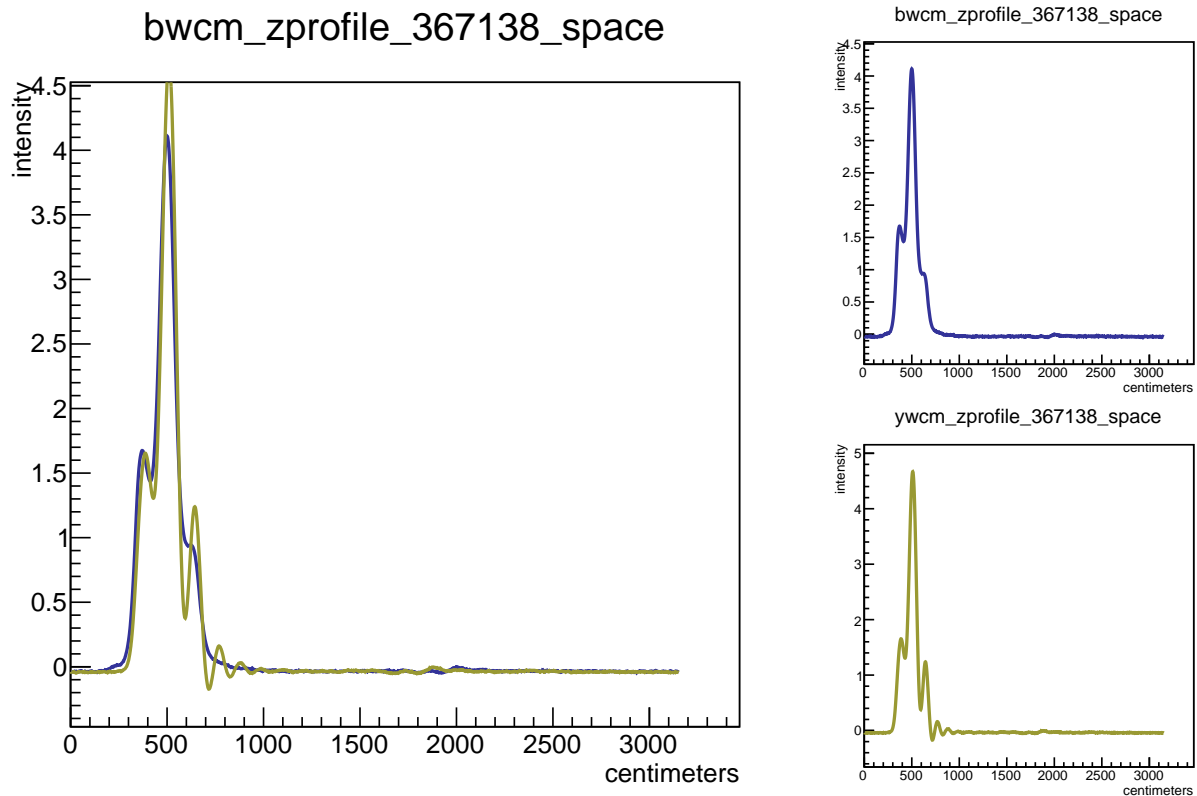
Figure 5.12: Left: the blue and yellow wall current monitor beam z-profiles. One can see the three beam buckets which make up one so-called "filled bunch". Bunches are approximately 1000 cm long, the entire profile passes the IR once every 106 nanoseconds, though most of the bunch is actually within a time envelope of approximately 35 nanosecons. The panes on the right show the blue beam (top) and the yellow beam (bottom).
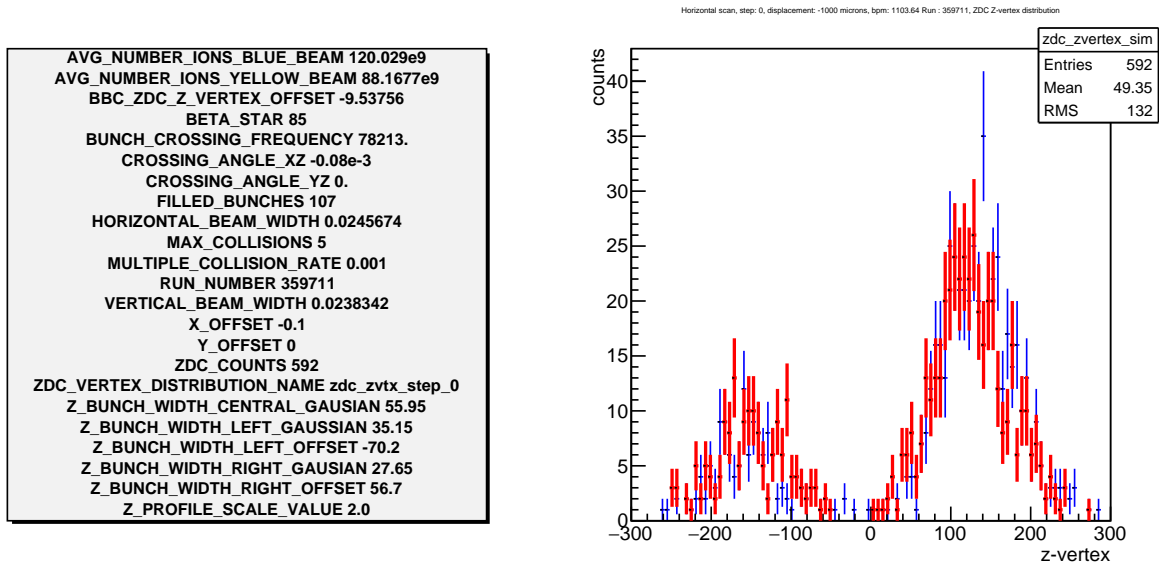
Figure 5.13: Here is the starting point for simulating the -1000 micron horizontal scan step from run 359711. We see good matching between simulation and data. Now we can proceed from this parameter configuration to calculating the best set of configuration parameters.

5.3.1   Hourglass Simulation Parameter Space

I systematically explored the hourglass parameter space to try and determine the best set of intial parameters to use to configure the starting point for the brute force regression. An example is seen in Figure **??**.

By running the simulation with extreme variations in the parameters, systematically, I identified how each parameter tends to affect the z-vertex profile. The following parameters map to the following z-profile behavior:

- $\theta_{XZ} \rightarrow$ Asymmetry in peak heights

- Beam Displacement / $\sigma x, y \rightarrow$ Peak Separation

- ZDC yield (not shown) $\rightarrow$ Peak Scaling

Also note that scaling the beam widths OR changing the displacement will change the total amount of overlapping beam. It was also determined that we cannot observe the effects of vertical-beam width scaling or YZ crossing angle during a horizontal beam displacement, similarly in the horizontal case.

Detailed slides on this study were presented to the Spin PWG on 11 November 2015, the slides are attached to the Agenda under speaker "Mike Beaumier".

Chapter 6

Multiple Collisions

This is the chapter on MultipleCollisions

Chapter 7

Acknowledgements

Though I am sure I will miss people, I feel it is important to at least try to thank those who have significantly contributed to this analysis, and my development as a graduate student, because I was a fresh, green grad student when Is tarted this analysis, and am now nearing the completion of my PhD. So, finishing this analysis is quite personally significant, for me.

I thank my adviser, Ken Barish, who has financially supported me throughout graduate school, and allowed me to fully pursue research with few distractions. He has put me into contact with experts which have helped me immeasurably, and given me lots of insight as to the inner mechanics of how a large collaboration works, how to manage graduate students and run a research group, and has given me plenty of freedom to develop personally and professionally according to my interests, without sacrificing guidance along the way towards completing my analyses and PhD.

I would like to thank Oleg Eyser, who I'm sure could find better uses for his time than teaching fresh graduate students the basics of C++ programming and root, but still made sure I was on track early in my work on this analysis.

I would like to thank Richard Hollis, who has been kind, patient, and good spirited in supporting the many students of my group in their work and struggles with tough problems. Richard has always managed to find time to look over somebody's code, prepare brief examples, and tools for more efficient analysis.

I'd also like to thank Joe Seele, Martin Purshke, John LeJoie, Chris Pinkenburg and John Koster, for their technical assistance. Martin was instrumental in helping to solve the issue of recovering time-stamps which allowed us to time-order this analysis, using scaler events to calculate live-time for various triggers, and many other nitty gritty details which only an expert at PHENIX software can help with. Joe was very patient with many of my questions regarding learning how to be a better programmer, without his help, I would still be running ROOT macros, instead of creating efficient, fast software libraries, extending my reach beyond just ROOT. Joe's help has allowed my analyses to become flexible and

Bibliography

[1] A Bazilevsky, R Bennett, A Deshpande, Y Goto, D Kawall, and J Seele, *Absolute luminosity determination using the vernier scan technique : Run4 6 Analysis and preliminary results at s = 62 . 4 GeV*, 2007. (document)

[2] S. Belikov, G.Bunce, M. Chiu, B. Fox, Y. Goto, T. Kawabata, N. Saito, M. Tannenbaum, and K. A. Drees, *Determination of the Absolute Luminosity for the Proton-Proton Data at 200 GeV Recorded by PHENIX during RHIC Run-02*, 2003. (document)

[3] Amaresh Datta and Dave Kawall, *σ BBC using Vernier Scans for 500 GeV pp Data in Run09 List of Figures*, 2010. (document)

[4] A Drees, *Analysis of Vernier Scans during RHIC Run-13 (pp at 255 GeV / beam)*, **13** (2013), 1–18. 1, 2.1